JAERI-Research
95-067

# EVALUATION OF NUCLEAR DATA OF $^{244}Pu$ AND $^{237}Pu$

October 1995

Tsuneo NAKAGAWA and Valentin A. KONSHIN*

日本原子力研究所
Japan Atomic Energy Research Institute

本レポートは，日本原子力研究所が不定期に公刊している研究報告書です。
入手の問合わせは，日本原子力研究所技術情報部情報資料課（〒319-11 茨城県那珂郡東海村）あて，お申し越しください。なお，このほかに財団法人原子力弘済会資料センター（〒319-11 茨城県那珂郡東海村日本原子力研究所内）で複写による実費頒布をおこなっております。

This report is issued irregularly.
Inquiries about availability of the reports should be addressed to Information Division, Department of Technical Information, Japan Atomic Energy Research Institute, Tokai-mura, Naka-gun, Ibaraki-ken 319-11, Japan.



編集兼発行　日本原子力研究所
印　　刷　㈱原子力資料サービス

# Evaluation of Nuclear Data of $^{244}$Pu and $^{237}$Pu

Tsuneo NAKAGAWA and Valentin A. KONSHIN*

Department of Reactor Engineering
Tokai Research Estabilshment
Japan Atomic Energy Research Institute
Tokai-mura, Naka-gun, Ibaraki-ken

(Received October 2, 1995)

The evaluation of nuclear data for $^{244}$Pu and $^{237}$Pu was made in the neutron energy region from $10^{-5}$ eV to 20 MeV. For the both nuclides, the total, elastic and inelastic scattering, fission, capture, (n, 2n) and (n, 3n) reaction cross sections were evaluated on the basis of theoretical calculation. The resonance parameters were given for $^{244}$Pu. The angular and energy distributions of secondary neutrons were also estimated for the both nuclides. The results were compiled in the ENDF－5 format and will be adopted in JENDL Actinoid File.

Keywords: Nuclear Data, Plutonium－244, Plutonium－237, Evaluation, JENDL Actinoid File, ENDF Format.

---

* Research Fellow (October 1993－April 1995)

# $^{244}$Puと$^{237}$Puの核データ評価

日本原子力研究所東海研究所原子炉工学部
中川 庸雄・Valentin A.KONSHIN*

（1995年10月2日受理）

中性子エネルギー$10^{-5}$eV～20MeVにおける$^{244}$Puと$^{237}$Puの核データ評価を行った。理論計算をもとに，両核種の全断面積，弾性散乱と非弾性散乱断面積，核分裂断面積，捕獲断面積及び（n，2n）と（n，3n）反応断面積を評価した。$^{244}$Puに対しては，分離共鳴パラメータを評価した。また，反応後に放出される二次中性子の角分布とエネルギー分布も推定した。結果は，ENDF－5フォーマットで編集されており，JENDLアクチノイドファイルに採用される予定である。

東海研究所：〒319-11 茨城県那珂郡東海村白方白根2－4
* リサーチフェロー（1993年10月～1995年4月）

# Contents



# 目　　次

## 1. Introduction

Nuclear data of minor actinoids are important for the fuel cycle study. In Japan, OMEGA project is being promoted to study a way of management of high level waste from nuclear energy plants. It is needed to precisely estimate the amount of minor actinoids in the reactors. A TRU burner reactor[1] is one of options for transmutation of minor actinoids to other nuclides with shorter half-life or stable nuclides. This reactor will have a harder neutron spectrum, and large amount of minor actinoids will be loaded in the reactor. Therefore accurate nuclear data are required even for minor actinoids. To meet the requirement for the minor actinoid nuclear data, "JENDL Actinoid File"[2] is under preparation at the Nuclear Data Center in Japan Atomic Energy Research Institute. In this file, evaluated neutron induced reaction data will be provided for about 90 nuclides including main nuclides ($^{232}$Th, $^{233}$U, $^{235}$U, $^{238}$U, $^{239}$Pu, $^{240}$Pu and $^{241}$Pu) and minor actinoids with a half-life longer than 1.0 day. In the present work, the nuclear data evaluation was made for $^{244}$Pu and $^{237}$Pu in order to store the data in the JENDL Actinoid File.

The nuclide $^{244}$Pu disintegrates with the half-life of $8.26\times10^{7}$ years and $^{237}$Pu with the half-life of 5.17 days. The nuclide $^{244}$Pu decays with $\alpha$ emission of 99.875 % and spontaneous fission of 0.125 %. In the case of $^{237}$Pu, the $\alpha$ decay is only 0.0033 % and the rest is the electron capture. Evaluated data for the both nuclides are available in ENDF/B-VI[3] and JEF-2.[4] However the same data are stored in the both files because they adopted the data from the evaluation made by Mann et al.[5] for ENDF/B-V. Experimental data exist only for the fission cross section and resonance parameters of $^{244}$Pu as is described in Chapter 2. The present evaluation of nuclear data of $^{244}$Pu is described in Chapter 2, and that of $^{237}$Pu in Chapter 3. The results of the present work have been compiled in the ENDF format, and will be adopted in the JENDL Actinoid File.

## 2. Evaluation of $^{244}$Pu Data

### 2.1 Resonance parameters

Auchampaugh et al.[6] measured the fission cross section by using a nuclear explosion (Physics 8) as a neutron source, and obtained information on the resolved resonance parameters below 285 eV. They used the TOF method with a flight path of 245.45 m and a Pu oxide sample with 99.06 % $^{244}$Pu, and deduced the capture areas for the 13 levels.

Their results were adopted in the recommendation made by Mughabghab[7]. In the present work, the recommendation of Mughabghab was used by assuming an average capture width of 20 meV. The fission width was determined so as to reproduce the integrated fission cross sections around each resonance peak measured by Auchampaugh et al. The numerical data were taken from EXFOR.[8] Thus obtained fission widths are almost 1/1000 of the capture widths, but for some resonances the ratio is quite different from 1/1000. The results are listed in Table 2.1. All the levels were assumed to belong to s-wave resonances. The effective scattering radius of 9.33 fm was obtained from the shape elastic scattering cross section calculated with the optical model. The Breit-Wigner multi-level formula was applied. The fission cross section calculated from the resonance parameters are compared with the experimental data of Auchampaugh et al. in Fig. 2.1.

Thermal cross sections and resonance integrals are listed in Table 2.2. In the calculation of resonance integral, integration was made between 0.5 eV and 20 MeV considering cross sections above the resonance region. The thermal capture cross section obtained from the resonance parameters is in good agreement with the experimental data. However the calculated resonance integral of capture cross section is larger than the experiments. ENDF/B-VI gives too large capture resonance integral. For the fission cross section, no experimental data are existing at the thermal energy and for the resonance integral.

### 2.2 Cross sections above Resonance Region

#### 2.2.1 Theoretical calculation

In the energy region above 290 eV, experimental data exist only for the fission cross section. Therefore, the fission cross section was determined mainly on the basis of the experimental data and the other cross sections were taken from theoretical calculations with ECIS[9], STAPRE[10] and CASTHY[11] to obtain a complete set of the cross sections up to 20 MeV.

ECIS Calculation

The code ECIS was used for the calculation of the total cross section, the shape elastic scattering cross section, angular distributions of elastically scattered neutrons and of the direct component of the inelastic scattering cross section. The deformed optical potential parameters used in the present work have the following values:

$V_R = 46.03 - 0.3E$, $0 \le E \le 20$ MeV

$W_D^{surf} = 3.05 + 0.4E$, $0 \le E \le 10$ MeV

$7.05 - 0.082(E-10)$, $10 \le E \le 20$ MeV

$W_V^{vol} = 8.0 \times \{1+\exp[-(E-50)/10]\}^{-1}$, $0 \le E \le 20$ MeV

$V_{SO} = 6.2$

$r_R = 1.26$, $a_R = 0.63$

$r_D = 1.26$, $a_D = 0.52$

$r_{SO} = 1.12$, $a_{SO} = 0.47$

$\beta_2 = 0.204$, $\beta_4 = 0.051$

These parameters were determined by Konshin considering Refs. 12 and 13. The introduction of the volume absorption term seems to lead to a better agreement with actinide experimental data for the total cross section in the energy region around 20 MeV and for the angular distributions of the inelastically scattered neutrons on low lying levels.

The ECIS calculation was made in the energy range from 10 keV to 20 MeV.

STAPRE Calculation

The STAPRE code was used for calculations of the fission cross section, (n,2n) and (n,3n) reaction cross sections and the total inelastic scattering cross section. The neutron transmission coefficients for these calculations were obtained using the ECIS code. The level densities were calculated with a phenomenological model proposed by Ignatyuk et al.[14] taking into account shell, superfluid and collective effects. The hard component of neutron scattering spectra was parameterized using the experimental data for $^{238}U$ in the 6 – 14.7 MeV region and the matrix element for the pre-equilibrium reaction stage description $M^2 = 10/A^3$ MeV$^2$.

The most critical values for a good description of experimental data on the fission cross section within the framework of the model used in STAPRE are reliable neutron transmission coefficients, a tested pre-equilibrium neutron emission contribution and fission barrier parameters. The fission barrier parameters $E_f^A$ and $E_f^B$ used were the following:

| nuclide | $E_f^A$(MeV) | $E_f^B$(MeV) |
|---|---|---|
| $^{245}$Pu | 5.75 | 5.40 |
| $^{244}$Pu | 5.50 | 5.20 |
| $^{243}$Pu | 6.00 | 5.70 |
| $^{242}$Pu | 5.60 | 5.35 |

The discussions on the fission barrier parameters are given elsewhere.[15)]

CASTHY Calculation

The ECIS code dose not consider the compound process, and the STAPRE code does not calculate inelastic level excitation cross sections. Therefore, the cross sections due to the compound process were calculated by using a statistical model code CASTHY. The optical potential parameters used are the following ones.[16)]

$V_R$ = 45.036 − 0.3 E (MeV), $r_R$ = 1.256, $a_R$ = 0.626 (fm)

$W_D$ = 4.115 + 0.4 E (MeV), $r_D$ = 1.260, $a_D$ = 0.555+0.0045E (fm)

$V_{SO}$ = 7.5 (MeV), $r_{SO}$ = 1.256, $a_{SO}$ = 0.626 (fm)

The level density parameters for Gilbert−Cameron's formula were determined from average level spacing of measured resonances[7)] and staircase plots of low−lying excited levels taken from ENSDF. Paring energies were assumed as follows[17)]:

$\delta$ = $2\times12/\sqrt{A}$ for even−even nuclides,

$12/\sqrt{A}$ for odd nuclides,

0.0 for odd−odd nuclides.

Other parameters of level density were determined so as to reproduce the staircase plot of excited levels. Obtained results are given in Table 2.3. The level scheme of $^{244}$Pu listed in Table 2.4 was adopted from ENSDF (Evaluated Nuclear Structure Data File).

In the CASTHY calculation, the fission, (n,2n) and (n,3n) reaction cross sections were considered as competing processes.

### 2.2.2 Compilation of cross section data

These results of the theoretical calculations were compiled as follows in the ENDF−5 format.

1) Total Cross Section

Above 10 keV, the ECIS calculation was adopted. Below 10 keV, it was obtained as

a sum of the fission, capture and elastic scattering cross sections.

2) Elastic Scattering Cross Section

Above 4.5 MeV, the ECIS calculation was adopted. Between 10 keV and 4.5 MeV, the cross section was obtained by subtracting a sum of partial cross sections from the total cross section. In the low energy region, the present ECIS calculation gives too small elastic scattering cross sections since the compound elastic process is not included in the calculation. Below 10 keV, the cross section was assumed to be a constant value of 13.36 b which was the value obtained at 10 keV by subtraction of partial cross sections from the total cross section.

3) Inelastic Scattering Cross Sections

The cross sections due to the compound process were calculated with CASTHY. The contributions from the direct process were calculated with ECIS and added to the CASTHY results. The continuum inelastic scattering cross section calculated with CASTHY was too large in the energy region above 4.5 MeV because the optical model parameters used in the CASTHY calculation were not perfectly consistent with those for the ECIS calculation. The continuum inelastic scattering cross section in this energy range was replaced with the values obtained by subtracting a sum of the elastic and direct inelastic scattering cross section, fission, (n,2n), (n,3n) and capture cross sections from the total cross section calculated with ECIS.

The consistency of cross sections were kept by adopting adjusted values for the elastic scattering cross section in the energy range below 4.5 MeV, and by the continuum inelastic scattering cross section above 4.5 MeV.

4) (n,2n) and (n,3n) Reaction Cross Sections

They were calculated with STAPRE. The (n,4n) reaction cross section was ignored because its threshold energy of 17.44 MeV is high and the cross section is not important for the fuel cycle study.

5) Fission Cross Section

There are six sets of experimental data.

Auchampaugh et al.[6)]

They measured the fission cross section relative to the $^{6}Li(n,t)$ and $^{235}U$ fission cross sections in the neutron energy region from 20 eV to 10 MeV by using a nuclear explosion as a neutron source. Their analysis of resonance parameters were adopted in the present work.

Fomushkin et al.[18)]

The fission cross section was measured with EhG－5 electrostatic accelerator in the energy range from 500 keV to 2.5 MeV. The measurements were made relatively to the $^{235}U$ fission cross section.

Gokhberg et al.[19)]

The measurement was performed in the energy range from 0.28 to 1.8 MeV with an electrostatic accelerator. To obtain the $^{244}Pu$ fission cross section, the $^{239}Pu$ fission cross section of 1.77 barns at 1.03 MeV was used.

Behrens et al.[20)]

The fission cross section ratio to $^{235}U$ was measured in the energy range from 0.1 to 30 MeV using 100－MeV linear accelerator at Lawrence Livermore Laboratory and ionization fission chambers.

Khan et al.[21)]

They measured the fission cross section at 14.8 MeV relatively to the $^{239}Pu$ fission cross section. Using the $^{239}Pu$ fission cross section of 2.52 barns, the fission cross section of 0.91±0.09 barn was obtained. This cross section is in good agreement with a $Z^{4/3}/A$ systematics of 14 MeV fission cross section.

Moore et al.[22)]

The fission cross section was measured in the energy range from 1 keV to 8 MeV relative to $^{235}U$ fission cross section by using CBNM linear accelerator. The effective resolution was 0.4 ns/m. From the evaluated cross section in ENDF/B－V and the measured data, the $^{244}Pu$ fission cross section was obtained.

These data are shown in Fig. 2.2. Since Behrens et al. reported only ratio data, the fission cross section of $^{235}U$ evaluated for JENDL－3.2 was used to get the $^{244}Pu$ fission cross section. The data of Auchampaugh et al., Fomushkin et al., Gokhberg et al. and Khan et al. are smaller than those of Moore et al. and Behrens et al. Figure 2.2 shows also the values calculated with STAPRE. It is seen that STAPRE calculation is in good agreement with the

experimental data of Moore et al. and Behrens et al. in the energy region from 2 to 20 MeV. Below 1 MeV, the calculation might be too small. The STAPRE calculation around 1 MeV was not made, since energies specified by input data are shifted by STAPRE, and it was difficult to get cross sections around 1 MeV.

In the present work, the results of the STAPRE calculation was adopted above 8 MeV. Below 8 MeV, a smooth curve was determined by eye－guiding of the experimental data of Moore et al. and Auchampaugh et al. In the energy region above 300 keV. the data of Moore et al. were adopted, because they were the most recent experimental data. Below 300 keV, the data of Auchampaugh et al. were used. Below 10 keV, the data were smoothed out with an energy resolution of 0.3×E where E is a neutron energy and a factor of 0.3 was determined to get an adequate structure of smoothed cross section. The fission cross section in this energy range was determined from thus obtained smooth curve. Figure 2.3 is a comparison of the present evaluation with the experimental data.

6) Capture Cross Section

This cross section was calculated with CASTHY. The average capture width of 20 meV[7] and the average level spacing of 17 eV[7] were assumed. In the MeV region, direct capture cross section was assumed to be about a few mb (3.0 mb at 4 MeV and 4.0 mb at 20 MeV) and added to the CASTHY calculation.

## 2.3 Angular Distributions of Secondary Neutrons

The angular distributions of elastically scattered neutrons were calculated with ECIS. Those of inelastically scattered neutrons were obtained by the CASTHY calculation for the compound process and by the ECIS calculation for the direct process. Both were summed up to the final results. For the levels above 957 keV, only the compound process was considered.

The angular distributions of neutrons from the fission, (n,2n) and (n,3n) reactions were assumed to be isotropic in the laboratory system.

## 2.4 Energy Distributions of Secondary Neutrons

For the (n,2n), (n,3n) and continuum inelastic scattering, the energy distributions of secondary neutrons were obtained by STAPRE. The fission spectrum was assumed to be the evaporation spectrum with the nuclear temperature of 1.347 MeV obtained from systematics

given by Smith et al.[23]

## 2.5 Neutrons per Fission

The number of delayed neutrons per fission ($\nu_d$) was estimated with a systematics of Manero and Konshin.[24] The number of delayed neutrons is 0.03 in the thermal energy region and 0.019 in the MeV region. The energy range from 4 to 7 MeV was assumed to be a transient region of the two values. The six group decay constants were assumed to be the same as those of $^{242}$Pu evaluated by Brady and England.[25]

The prompt neutrons ($\nu_p$) was determined on the basis of experimental data for $^{240}$Pu and $^{242}$Pu:

$$\nu_p = 2.79 + 0.163 \times E(MeV).$$

This is close to $\nu_p = 2.688 + 0.184 \times E(MeV)$ obtained from Howerton's systematics.[26]

## 2.6 Discussion on $^{244}$Pu Data

The cross sections obtained in the present evaluation are compared with those in ENDF/B－VI in Figs. 2.4 to 2.9. The cross sections in the resolved resonance region in these figures are averaged in quarter lethargy intervals. ENDF/B－VI gives hypothetical resolved resonances below 249 eV and unresolved resonance parameters at energies between 249 eV and 10 keV. Large discrepancies are found in the resonance region except the thermal energy region. The fission cross section in ENDF/B－VI is zero at low energies, while the present evaluation gives small values on the basis of the experimental data. Above 100 keV, the both evaluations are almost the same. ENDF/B－VI adopted the data of Behrens et al. which are slightly smaller than the data of Moore et al. There are also rather large discrepancies in the capture, inelastic scattering, (n,2n) and (n,3n) reaction cross sections, because of no available experimental data.

The angular distributions of elastically scattered neutrons are shown in Fig. 2.10. The present results are almost the same as ENDF/B－VI. Figures from 2.11 to 2.19 are the angular distributions of inelastic scattering neutrons at 2 and 10 MeV. On the figure of 2 MeV data, contributions from the direct process calculated with ECIS are shown together with the present result which is a sum of direct and compound processes.

Figure 2.20 displays the energy distributions of (n,2n) reaction neutrons at the incident energy of 10 MeV. ENDF/B－VI adopted the evaporation spectra, and the present evaluation the STAPRE calculation. The same tendency as the (n,2n) reaction is found in the energy

distributions of continuum inelastic scattering neutrons shown in Fig. 2.21. The fission neutron spectra in Fig. 2.22 are almost the same each other.

## 3. Evaluation of $^{237}$Pu Data

### 3.1 Cross sections in the thermal region

Available experimental data is only the fission cross section measured by Gindler et al.[31] They used the thermal column of the Argonne heterogeneous heavy-water reactor, CP-5, and obtained the cross section of 2500±500 b. CINDA[32] stores an index line of experiment made by Hulet et al.[33] with the cross section of 2200 b. However, this is not in published reports. Mughabghab[7] recommended the thermal cross section of 2455±295 b. We adopted this value as the cross section at 0.0253 eV. The ratio of fission cross section to capture cross section was assumed to be the same as that in the keV region. The ratio in the keV region is about 1/5 as is described in the next section. Therefore, the capture cross section of 500 b at 0.0253 eV was adopted in the present work. Both cross sections were assumed to have a form of 1/v, and smoothly connected the cross sections at 1 eV. The adopted elastic scattering cross section is a constant of 11.5 b which was calculated at low energies with CASTHY as described in the next section. The total cross section was calculated as a sum of these cross sections.

No resonance parameters were given, because no experimental data were available for the resonance parameters and the level spacing estimated from level density parameters was so small that Doppler effects might not be important.

### 3.2 Cross sections above 1 eV

3.2.1 Theoretical calculation

In this energy range, no experimental data are available. Theoretical calculations of cross sections were made with ECIS, STAPRE and CASTHY.

ECIS Calculation

The total and shape elastic scattering cross sections, angular distributions of elastically and inelastically scattered neutrons and neutron transmission coefficients were calculated with ECIS in the energy range above 400 keV. An even-Z and odd-N nucleus $^{237}$Pu is difficult to analyze in terms of the coupled channel method, as it has a high spin of the ground state (7/2) and, besides, the K=7/2 and K=1/2 bands become mixed already at low energy (0.15 MeV) and the band mixing increases with the energy of the excited states. This is the evidence of nonaxial symmetric deformation and it seems questionable to assume a symmetric rotational model for the analysis of $^{237}$Pu. However this model has the advantage of making

the entire analysis of the neutron scattering on $^{237}$Pu easier.

The code ECIS was used in the energy range from 0.4 to 20 MeV (the symmetric rotational model for the low lying band K=7/2). Five levels of this band were considered coupled. In the ECIS code, it was not possible to take into account the second rotational band K=1/2 mixed with K=7/2. Coupled channel calculations for $^{237}$Pu were made using the following optical model parameters:

$V_R = 46.2 - 0.3E$, $0 \leq E \leq 20$ MeV

$W_D^{surf} = 3.05 + 0.4E$, $0 \leq E \leq 10$ MeV

$7.05 - 0.082(E-10)$, $10 \leq E \leq 20$ MeV

$W_V^{vol} = 8.0\times\{1+\exp[-(E-50)/10]\}^{-1}$, $0 \leq E \leq 20$ MeV

$V_{SO} = 6.2$

$r_R = 1.26$, $a_R = 0.63$

$r_D = 1.26$, $a_D = 0.52$

$r_{SO} = 1.12$, $a_{SO} = 0.47$

$\beta_2 = 0.220$, $\beta_4 = 0.07$

These parameters were determined by Konshin considering Refs. 12 and 13.

STAPRE Calculation

The code STAPRE was used for calculations of the fission cross section, (n,2n) and (n,3n) reaction cross sections and the inelastic scattering cross section. Neutron transmission coefficients for these calculations were provided by the ECIS code. The fission barrier parameters $E_f^A$ and $E_f^B$ used were the following:

| nuclide | $E_f^A$(MeV) | $E_f^B$(MeV) |
|---|---|---|
| $^{238}$Pu | 5.60 | 5.10 |
| $^{237}$Pu | 6.00 | 5.80 |
| $^{236}$Pu | 5.30 | 4.70 |
| $^{235}$Pu | 5.60 | 5.10 |

These parameters were determined so as to reproduce the experimental data of fission cross sections for neighboring nuclides and by considering their systematic trend.

CASTHY Calculation

CASTHY was used in order to calculate the inelastic scattering cross sections due to

the compound process and the capture cross section. The optical potential parameters used are listed in Chapter 2 with the following modification:

$$V_R = 44.7 - 0.3\ E\ (MeV).$$

This modification was made by assuming the total cross section in the keV region to have the same tendency of $^{239}Pu$ total cross section, and so as to reproduce such tendency.

The level density parameters for Gilbert－Cameron's formula were determined with the same way as $^{244}Pu$ evaluation. Obtained parameters are given in Table 2.3. Level scheme of $^{237}Pu$ listed in Table 3.1 that was adopted from ENSDF.

3.2.2 Compilation of cross section data

1) Total Cross Section

The adopted total cross section was the theoretical calculation with CASTHY in the energy range from 1 eV to 400 keV, and with ECIS above 400 keV.

2) Elastic Scattering Cross Section

Above 1 keV, this cross section was obtained by subtracting the sum of partial cross sections from the total cross section. Above 3 MeV, the results are essentially the same as ECIS calculation. Below 1 keV, it was assumed to be a constant value of 11.5 b which was obtained by the subtraction at 1 keV.

3) Inelastic Scattering Cross Sections

The direct inelastic process was calculated with ECIS to the 1st, 2nd, 5th and 8th levels. The direct inelastic scattering cross sections were added to the compound inelastic scattering cross sections calculated with CASTHY. Levels above 655 keV were assumed to be overlapping. The continuum inelastic cross section was calculated by means of CASTHY below 2 MeV, and by subtracting a sum of the elastic scattering cross section calculated with ECIS and the fission, (n,2n), (n,3n) and capture cross sections from the total cross section calculated with ECIS above 3 MeV. Thus determined cross sections were simply connected between 2 and 3 MeV.

4) (n,2n) and (n,3n) Reaction Cross Sections

They were calculated with STAPRE.

5) Fission Cross Section

Above 1 MeV, the results calculated by STAPRE were adopted. The shape of the cross section in the 100 keV region was assumed to be the same as that of $^{239}$Pu, and it was normalized to the fission cross section at 1 MeV. Below about 100 keV, since the resonance structure of $^{239}$Pu could not be adopted, the cross section was assumed to be $\sigma_{fis} = \sigma_R \times 0.85$ where $\sigma_R$ is the total reaction cross section calculated with CASTHY and the factor of 0.85 was estimated at 100 keV.

6) Capture Cross Section

The capture cross section was calculated with CASTHY. The average capture width of 47 meV and the average level spacing of 0.233 eV were assumed. The average capture width was estimated from the systematics by Malecki et al.[34], by Bondarenko and Urin[35] and by Gardner[36]. However, results of the CASTHY calculation that took into account of competing cross sections had unexpected shape around 1 MeV because the shape of the fission cross section based on the reaction cross section calculated with ECIS was inconsistent with the reaction cross section calculated with CASTHY. Therefore, the capture cross section adopted was calculated by CASTHY without competing process and normalized to the calculation with competing process at 10 keV. In the MeV region, the same amount of direct capture cross section as $^{244}$Pu was added to the CASTHY calculation.

### 3.3 Angular and Energy Distributions of Secondary Neutrons

The angular distributions of elastically scattered neutrons were calculated with ECIS above 400 keV, and with CASTHY below 400 keV. Those of inelastically scattered neutrons were obtained by the CASTHY for the compound precess and by ECIS for the direct process. The angular distributions of neutrons emitted from the fission, (n,2n) and (n,3n) reactions were assumed to be isotropic in the laboratory system.

The energy distributions of neutrons from the (n,2n), (n,3n) and continuum inelastic scattering were obtained by STAPRE. The fission neutron spectrum was assumed to be the evaporation spectrum with the temperature of 1.387 MeV that was obtained from the systematics given by Smith et al.[23]

### 3.4 Neutrons per Fission

The number of delayed neutrons per fission ($\nu_d$) was estimated with a systematics of

Manero and Konshin.[24] Estimated delayed neutron yield $\nu_d$ in the low energy region is 0.002 and that in the high energy region is 0.0014. The energy range from 4 to 7 MeV was assumed to be a transient area of these two values. The six group decay constants were assumed to be the same as those of $^{239}$Pu evaluated by Brady and England[25].

The number of prompt neutrons ($\nu_p$) was determined on the basis of experimental data for $^{239}$Pu:

$$\nu_p = 2.863 + 0.123 \times E(MeV).$$

This is close to $\nu_p = 2.9203 + 0.1420 \times E(MeV)$ obtained from Howerton's systematics.[26]

### 3.5 Discussion on $^{237}$Pu Data

The present evaluation is compared with evaluated data[5] in ENDF/B－VI. Table 3.2 is a list of thermal cross sections and resonance integral. Both evaluations give almost the same values.

The cross sections are shown in Figs. 3.1 to 3.7. The total and elastic scattering cross sections of the both evaluations are almost the same as shown in Figs. 3.1 and 3.2. Figures 3.3 and 3.4 are comparison of fission cross sections. Tendency of the cross section is the same in the both evaluations. However, ENDF/B－VI is larger than the present evaluation above 1 eV. As a result of these discrepancies, the resonance integral of ENDF/B－VI is about 30 % larger than the present evaluation. The capture cross sections in Fig. 3.5 are discrepant from each other around 1 eV and above 10 keV. The cross sections of inelastic scattering, and (n,2n) and (n,3n) reactions have remarkable discrepancies as shown in Figs. 3.6 and 3.7.

The graphs of the angular distributions of elastically and inelastically scattered neutrons and the energy distributions of neutrons emitted from (n,2n), continuum inelastic scattering and fission are shown in Figs. 3.8 to 3.15. Large discrepancies among the present results and ENDF/B－VI evaluations are found in the energy distributions of neutrons the (n,2n) reaction and continuum inelastic scattering. These discrepancies come from the discrepancies of their cross sections.

## 4. Conclusion

The nuclear data evaluation of $^{244}$Pu and $^{237}$Pu was made in the incident neutron energy range from $10^{-5}$ eV to 20 MeV. The available experimental data are quite limited, so the theoretical calculations were widely used. The parameters needed to the calculation was determined by systematic investigation for several nuclides around $^{244}$Pu and $^{237}$Pu. Especially the fission cross section calculated with the STAPRE code is reliable because the results of STAPRE are in good agreement with experimental data for several Pu isotopes. The present results will be stored in JENDL Actinoid File.

In order to improve the nuclear data of minor actinides, experimental data are quite important in particular for the fission, capture, (n,2n) cross sections and resolved resonance parameters in the low energy region. However, only the fission cross section of $^{244}$Pu in wide energy range and that of $^{237}$Pu at the thermal energy are available in the present work. Therefore, the uncertainties of the present results might be rather large except for the $^{244}$Pu fission cross section. New experimental data are deeply required to improve the present status of these nuclides.

**References**


1) Mukaiyama T., Takano H., Takizuka T., Ogawa T. and Osakabe M.: Proc. Int. Reactor Phys., Jackson Hole, 18–22 Sep. 1988, Vol. IV, p.369 (1988).
2) Nakagawa T., Fukahori T., Chiba and Kikuchi Y.: Proc. Int. Conf. and Technol. Exposition on Future Nuclear Systems, Seattle, 12–17 Sep. 1993, p. 467 (1993).
3) ENDF/B–VI, Evaluated Nuclear Data File / B, version VI second revision, BNL/NNDC (1993).
4) JEF–2, Joint Evaluation File, Version 2, second revision, OECD/NEA Data Bank (1992).
5) Mann F.M. and Schenter R.E.: "HEDL Evaluation of Actinide Cross Sections for ENDF/B–V," HEDL–TME 77–54 (1977).
6) Auchampaugh G.F., Farrell J.A. and Bergen D.W.: Nucl. Phys., A171, 31 (1971).
7) Mughabghab S.F.: "Neutron Cross Sections, Vol. 1, Part B," Academic Press Inc. (1984).
8) OECD NEA Data Bank: EXFOR, experimental nuclear database (1994).
9) Raynal J.: unpublished.
10) Uhl M. and Strohmaier B.: Report IRK–76/10 (1976).
11) Igarasi S. and Fukahori T.: "Program CASTHY – Statistical Model Calculation for Neutron Cross Sections and Gamma ray Spectrum –," JAERI 1321 (1991).
12) Konshin V.A.: Proc. of Workshop on Computation and Analysis of Nuclear Data Relevant to Nuclear Energy and Safety, Trieste, Italy, 10 Feb. – 13 Mar. 1992, World Scientific, p.775 (1993).
13) Haouat G., Lachkar J., Lagrange Ch., Jary J., Sigaud J. and Patin Y.: Nucl. Sci. Eng., 81, 491 (1982).
14) Ignatyuk A.V., Istekov K.K. and Smirenkin G.N.: Sov. J. Nul. Phys., 29, 450 (1979).
15) Konshin V.A.: "Consistent Clculations of Fast Neutron Induced Fission, (n,2n) and (n,3n) Cross–Sections for 71 Isotopes of Th, Pa, U, Np, Pu, Am, Cm, Bk and Cf," JAERI–Research 95–010 (1995).
16) Ignatyuk A.V., Klepatskii A.B., Maslov V.M. and Sukhovitskii E.Sh.: Sov. J. Nucl. Phys., 42, 360 (1985).
17) Mengoni A. and Nakajima Y.: "HERMES: A Personal–Computer Program for Calculation of the Fermi–Gas Model Parameters of Nuclear Level Density,"

JAERI-M 93-177 (1993).

18) Formushkin Eh.F., Maslennikov B.K., Novoselov G.F., Surin V.M. and Khodalev G.F.: "Nuclear Physics Research in the USSR," INDC(CCP)-100/U, p.9 (1977).

19) Gokhberg B.M., Dubrovina S.M. and Shigin V.A.: "Nuclear Physics Research in the USSR," INDC(CCP)-100/U, p.8 (1977).

20) Behrens J.W., Newbury R.S. and Magana J.W.: Nucl. Sci. Eng., 66, 433 (1978).

21) Khan N.A., Khan H.A., Gul K., Anwar M., Hussain G., Akber R.A., Waheed A. and Shaikh M.S.: Nucl. Instru. Meth., 173, 163 (1980).

22) Moore M.S., Budtz-Jørgensen, Knitter H.-H, Olsen C.E., Wattena J.A. and Weigmann H.: Proc. Int. Conf. Nuclear Data for Science and Technol., Antwerp, 6-10 Sep. 1982, p. 74 (1983).

23) Smith A., Guenther P., Winkler G. and Mcknight R.: "Prompt-Fission-Neutron Spectra of $^{233}U$, $^{235}U$, $^{239}Pu$ and $^{240}Pu$ relative to That of $^{252}Cf$," ANL/NDM-50 (1979).

24) Marero F. and Konshin V.A.: Atomic Energy Review, 10, 637 (1972).

25) Brady M.C. and England T.R.: Nucl. Sci. Eng., 103, 129 (1989).

26) Howerton R.J.: Nucl. Sci. Eng., 62, 438 (1977).

27) Butler J.P., Eastwood T.A., Collins T.L., Jones M.E., Rourke F.M. and Schuman R.P.: Phys. Rev., 103, 634 (1956).

28) Fields P.R., Pyle G.L., Inghram M.G., Diamond H., Studier M.H. and Manning W.M.: Nucl. Sci. Eng., 1, 62 (1956).

29) Schuman R.P.: IN-1317, p.54, Idaho Nuclear Corp. Report (1969), Data were taken from EXFOR 12510.

30) Druzhinin A.A., Krylov N.G., L'vov A.A., Odintsov Yu.M. and Sumatokhin V.L.: Sov. At. Energy, 46, 473 (1979).

31) Gindler J.E., Gray J. Jr. and Huizenga J.R.: Phys., Rev., 115, 1271 (1959).

32) CINDA-A (1935-1987), Vol. 5, The Index to Literature and Computer Files on Microscopic Neutron Data, IAEA (1990).

33) Hulet et al.: unpublished (1961).

34) Malecki H., Popov A.B. and Tshezak K.: Yad. Fiz., 37, 284 (1983).

35) Bondarenko V.I. and Urin M.G.: Yad. Fiz., 35, 675 (1982).

36) Gardner D.: Proc. Int. Conf. on Nuclear Cross-Sections and Technol., Vol.2, p.651 (1975).

Table 2.1 Resolved resonance parameters of $^{244}Pu$

| Resonance energy (eV) | Neutron width (meV) | Fission width (meV) |
|---|---|---|
| −6.0 | 1.558 | 0.02 |
| 4.0 | 0.026 | 0.02 |
| 30.7 | 2.2 | 0.022 |
| 40.3 | 1.03 | 0.022 |
| 53.5 | 0.80 | 0.025 |
| 64.3 | 15.5 | 0.021 |
| 87.6 | 3.2 | 0.013 |
| 102.0 | 43.0 | 0.020 |
| 128.0 | 3.0 | 0.020 |
| 161.0 | 2.10 | 0.012 |
| 185.0 | 31.0 | 0.018 |
| 191.0 | 3.20 | 0.023 |
| 227.0 | 300.0 | 0.020 |
| 233.0 | 4.1 | 0.020 |
| 285.0 | 61.0 | 0.020 |

$\Gamma_\gamma$ = 20 meV for all resonances.

R' = 9.33 fm.

All levels are s-wave resonances .

Table 2.2 Thermal cross sections and resonance integrals of $^{244}Pu$

(in barns)

| quantity | present | ENDF/B-VI | others | Ref. of others |
|---|---|---|---|---|
| $\sigma_{tot}$ | 12.036 | 11.465 | | |
| $\sigma_{ela}$ | 10.354 | 9.635 | | |
| $\sigma_{fis}$ | 0.0017 | 0.0 | | |
| $\sigma_{cap}$ | 1.680 | 1.830 | 1.7±0.1 | Mughabghab[7] |
| | | | 2.1±0.3 | Butler et al.[27] |
| | | | 1.5±0.3 | Fields et al.[28] |
| | | | 1.6±0.3 | Schuman[29] |
| $RI_{fis}$ | 5.07 | 4.73 | | |
| $RI_{cap}$ | 50.0 | 106. | 40.6±2.9 | Mughabghab[7] |
| | | | 35±7 | Schuman[29] |
| | | | 40±3 | Druzhinin et al.[30] |

Table 2.3 Level density parameters of Pu isotopes used in CASTHY calculation

| Nuclide | a($MeV^{-1}$) | T(MeV) | δ(MeV) | $E_x$(MeV) | α | $D_{obs}^{cal}$(eV) | $D_{obs}^{exp}$(eV) |
|---|---|---|---|---|---|---|---|
| $^{237}Pu$ | 30.94 | 0.389 | 0.779 | 4.2131 | 31.10 | 4.60 | － |
| $^{238}Pu$ | 31.68 | 0.394 | 1.556 | 5.1959 | 31.56 | 0.233 | － |
| $^{239}Pu$ | 30.35 | 0.394 | 0.776 | 4.2035 | 30.98 | 9.01 | 9.0±0.7 |
| $^{242}Pu$ | 32.60 | 0.380 | 1.543 | 5.0169 | 32.37 | 0.90 | 0.9±0.1 |
| $^{243}Pu$ | 32.66 | 0.355 | 0.7698 | 3.7248 | 32.49 | 15.5 | 15.5±1.7 |
| $^{244}Pu$ | 31.0 | 0.380 | 1.536 | 4.7720 | 31.74 | 2.34 | － |
| $^{245}Pu$ | 34.87 | 0.315 | 0.7667 | 3.1895 | 33.76 | 17.0 | 17±3 |

a: level density parameter

T: nuclear temperature

δ: pairing energy

$E_x$: connection energy of constant temperature model and Fermi gas model

α: spin－cutoff parameter

$D_{obs}$: s－wave average level spacing at neutron binding energy

Table 2.4 Level scheme of $^{244}Pu$

| Energy (keV) | spin | parity |
|---|---|---|
| 0.0 | 0 | + |
| 48.0 | 2 | + |
| 153.0 | 4 | + |
| 315.4 | 6 | + |
| 531.8 | 8 | + |
| 708.0 | 2 | + |
| 798.3 | 10 | + |
| 957.0 | 3 | － |
| 1015.0 | 2 | + |

The levels above 1.068 MeV were assumed to be overlapping.

Table 3.1 Level scheme of $^{237}Pu$

| Energy (keV) | spin | parity |
|---|---|---|
| 0.0 | 7/2 | − |
| 47.71 | 9/2 | − |
| 106.0 | 11/2 | − |
| 145.54 | 1/2 | + |
| 155.45 | 3/2 | + |
| 175.0 | 13/2 | − |
| 201.18 | 5/2 | + |
| 224.25 | 7/2 | + |
| 257.0 | 15/2 | − |
| 280.22 | 5/2 | + |
| 304.0 | 9/2 | + |
| 320.97 | 7/2 | + |
| 370.4 | 3/2 | + |
| 371.0 | 9/2 | + |
| 404.19 | 5/2 | + |
| 407.83 | 5/2 | + |
| 438.41 | 7/2 | + |
| 453.2 | 7/2 | + |
| 473.5 | 7/2 | + |
| 486.0 | 9/2 | + |
| 513.0 | 9/2 | + |
| 545.0 | 1/2 | − |
| 582.0 | 5/2 | − |
| 591.0 | 3/2 | − |

The levels above 655 keV were assumed to be overlapping.

Table 3.2 Thermal cross sections and resonance integrals

(in barns)

| quantuty | present | ENDF/B-VI | others | Ref. of others |
|---|---|---|---|---|
| $\sigma_{tot}$ | 2966.5 | 2651.7 | | |
| $\sigma_{ela}$ | 11.50 | 11.73 | | |
| $\sigma_{fis}$ | 2455.0 | 2100.0 | 2455±295 | Mughabghab[7] |
| | | | 2500±500 | Gindler et al.[31] |
| | | | 2200 | Hulet et al.[33] |
| $\sigma_{cap}$ | 500.0 | 540.0 | | |
| $RI_{fis}$ | 816 | 1085 | | |
| $RI_{cap}$ | 142 | 190 | | |

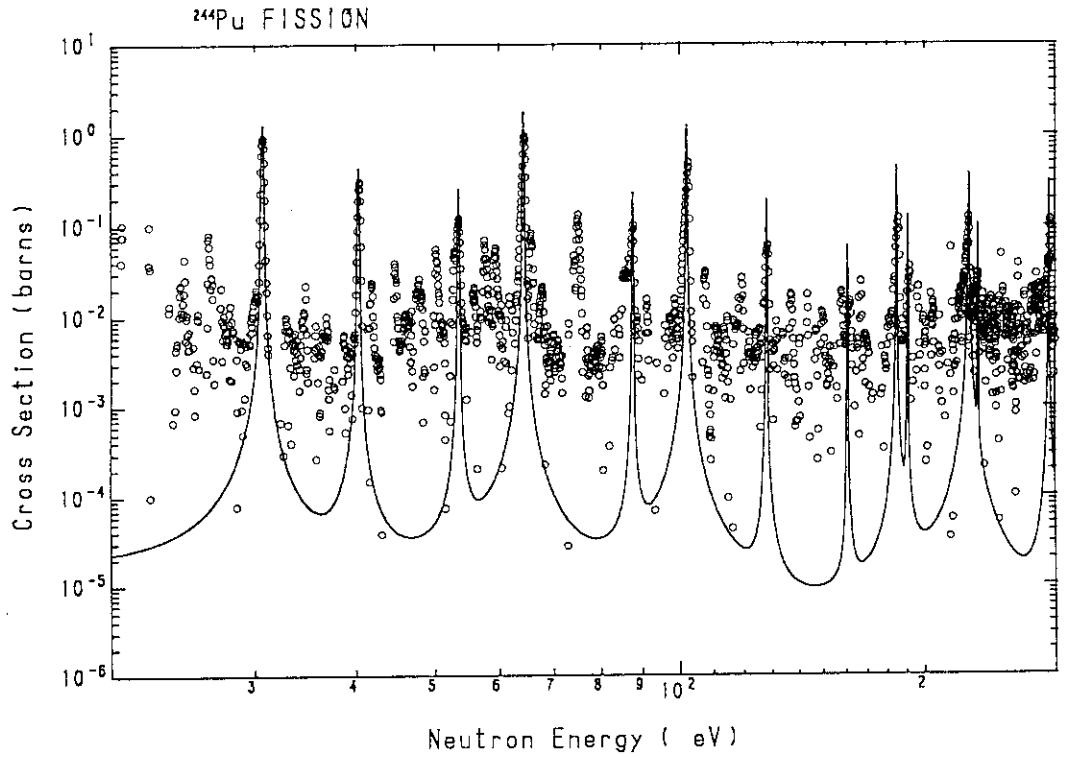


Fig.2.1 Fission cross section in the resolved resonance region. The experimental data were measured by Auchampaugh et al.[6] . Solid curve shows the cross section calculated from the resonance parameters taking account of Doppler effect at 300 K. Peaks not followed by the solid curve are due to impurities in the sample.

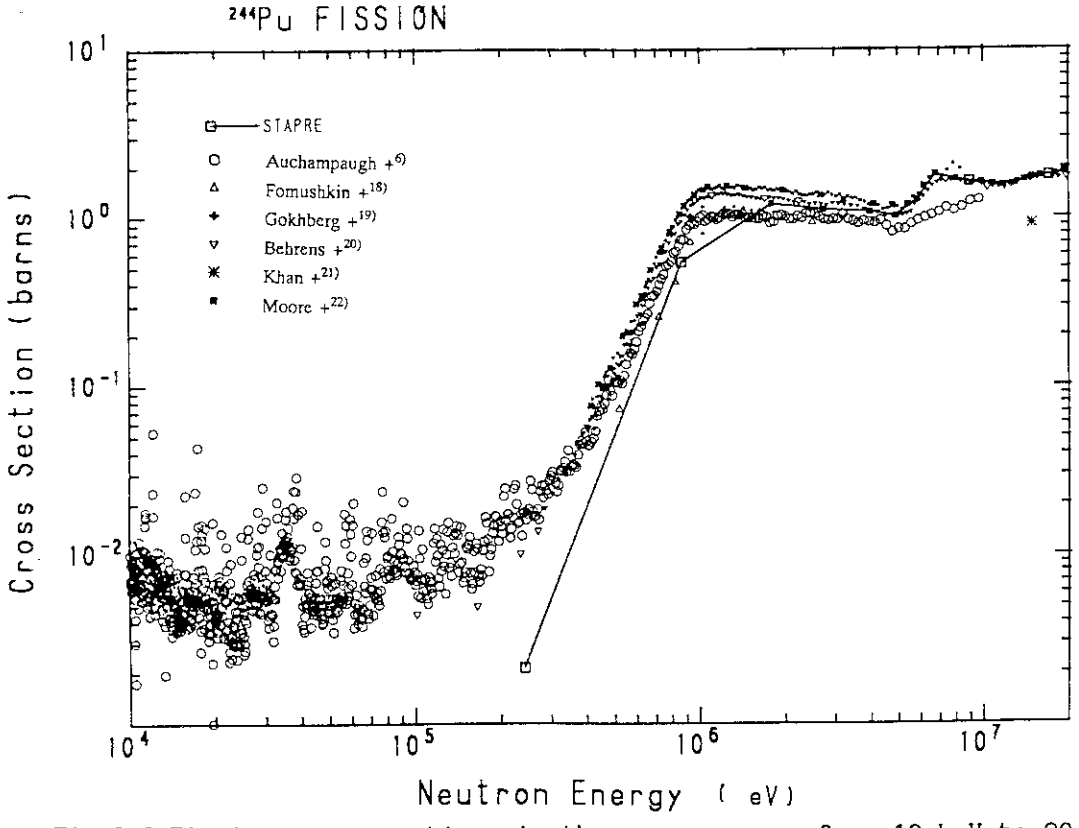


Fig.2.2 Fission cross sections in the energy range from 10 keV to 20 MeV. Squares are results of STAPRE calculation, and they are simply connected with a solid line.

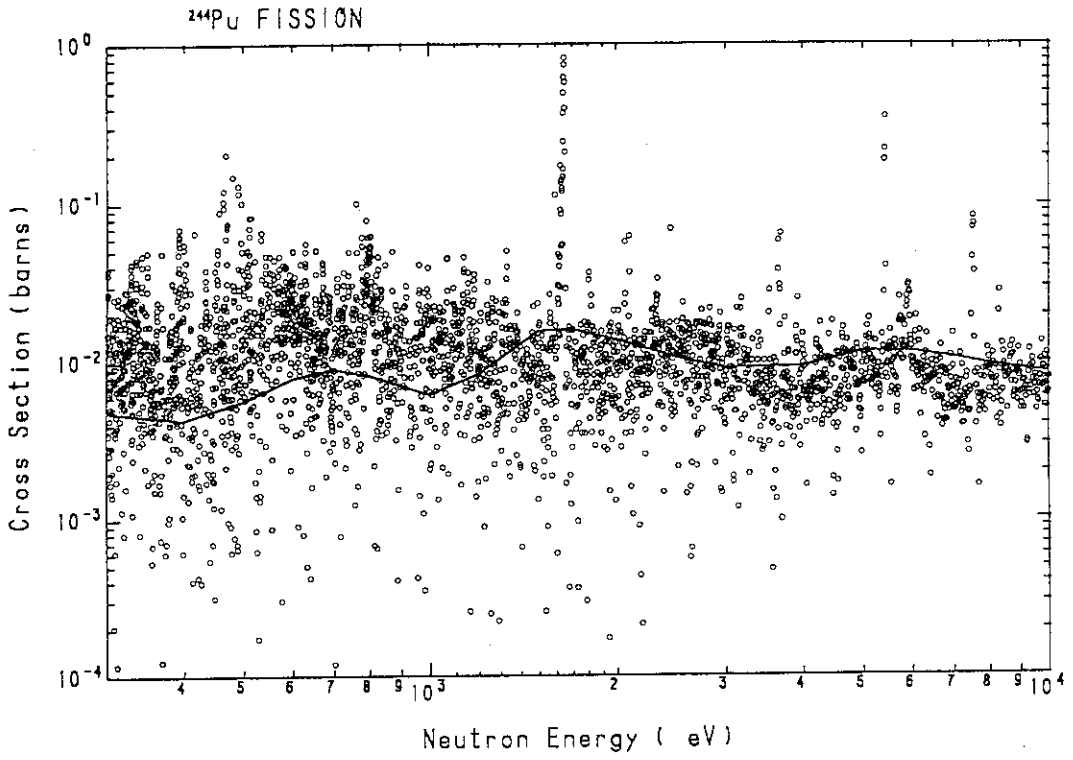


Fig.2.3(a) Comparison of evaluated fission cross section with the experimental data[6].

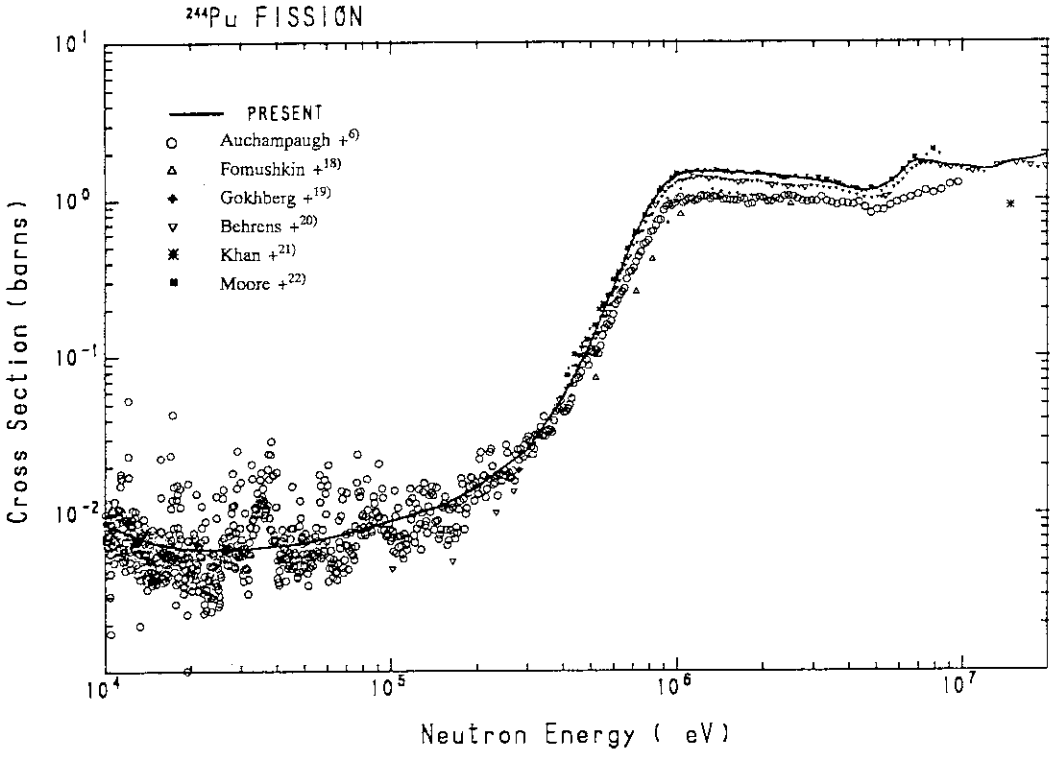


Fig.2.3(b) Comparison of evaluated fission cross section with the experimental data.

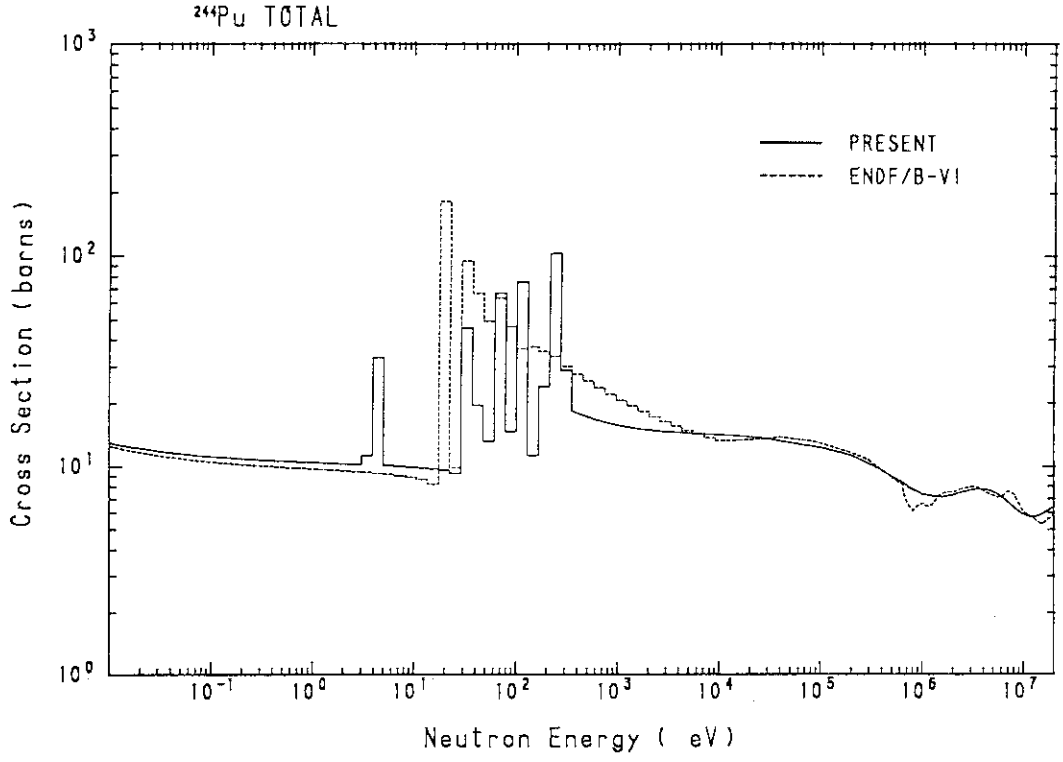


Fig.2.4 $^{244}$Pu total cross section

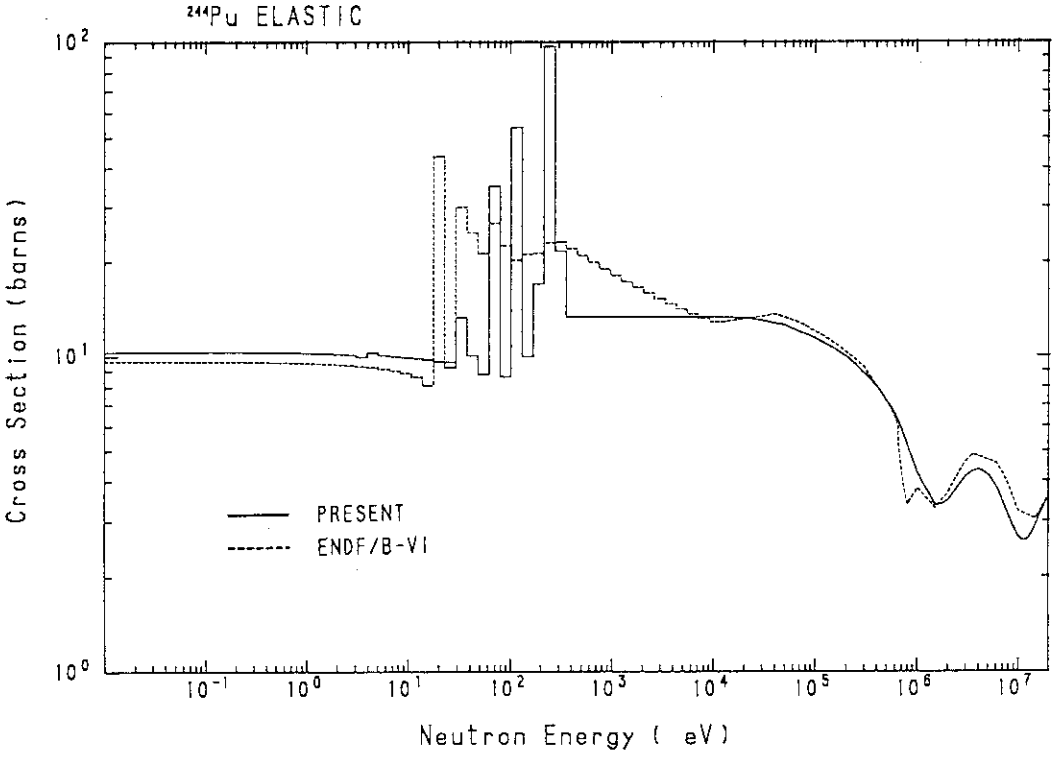


Fig.2.5 $^{244}$Pu elastic scattering cross section

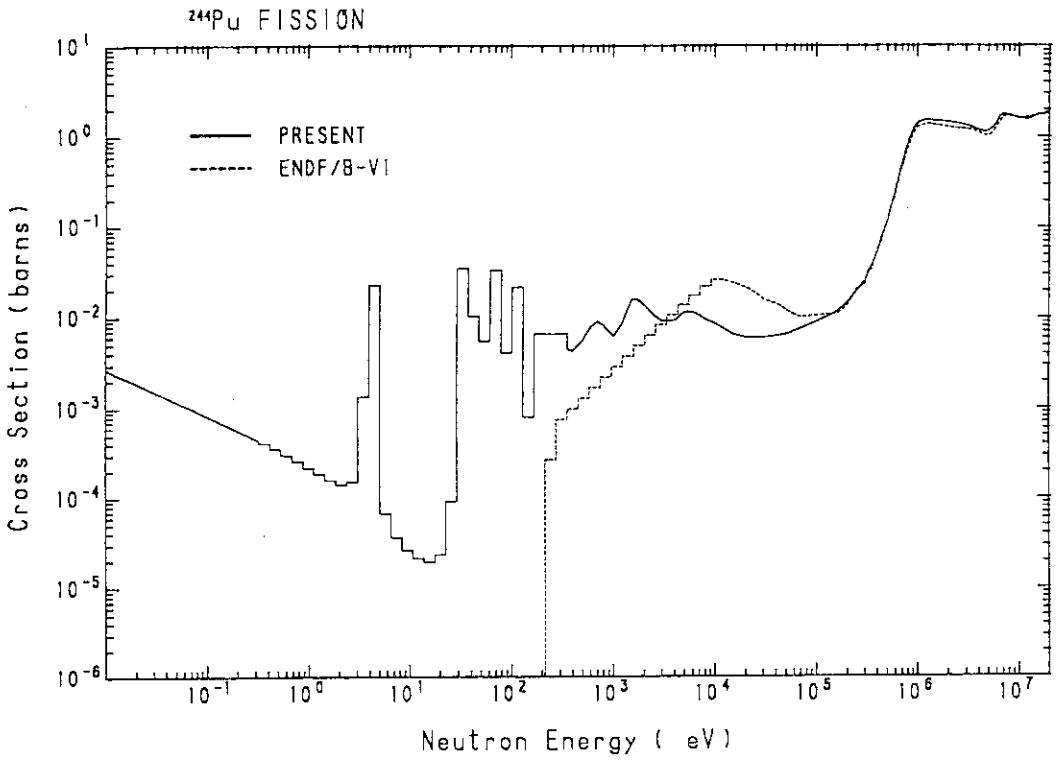


Fig.2.6 $^{244}$Pu fission cross section

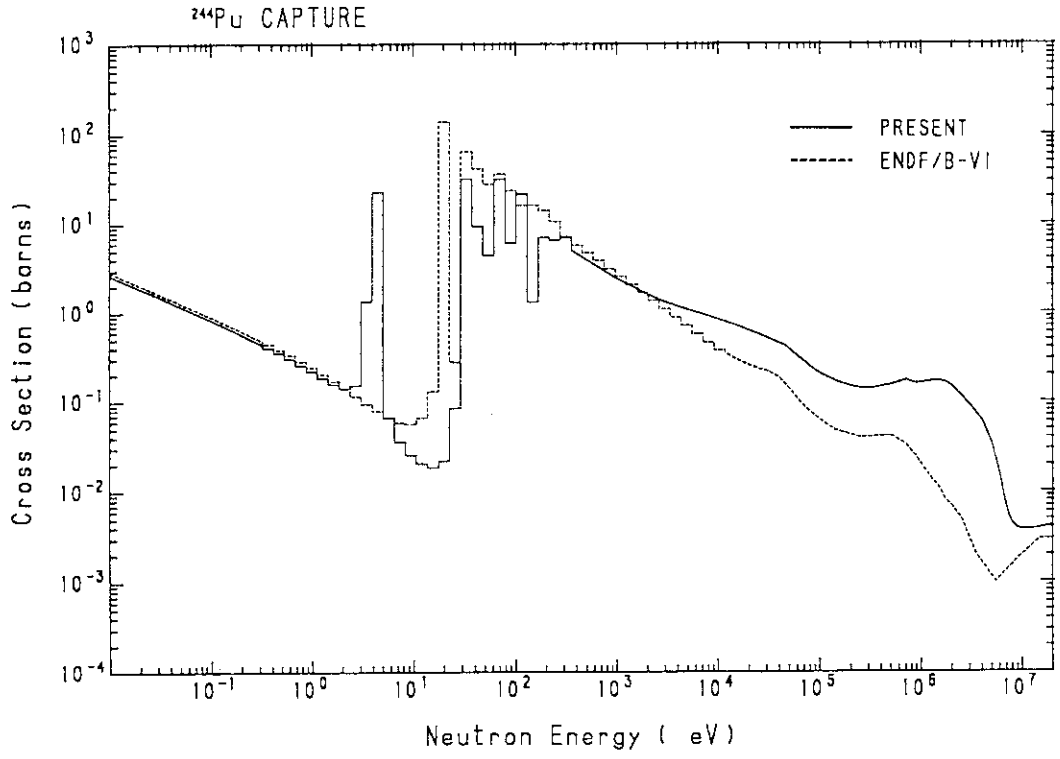


Fig.2.7 $^{244}$Pu capture cross section

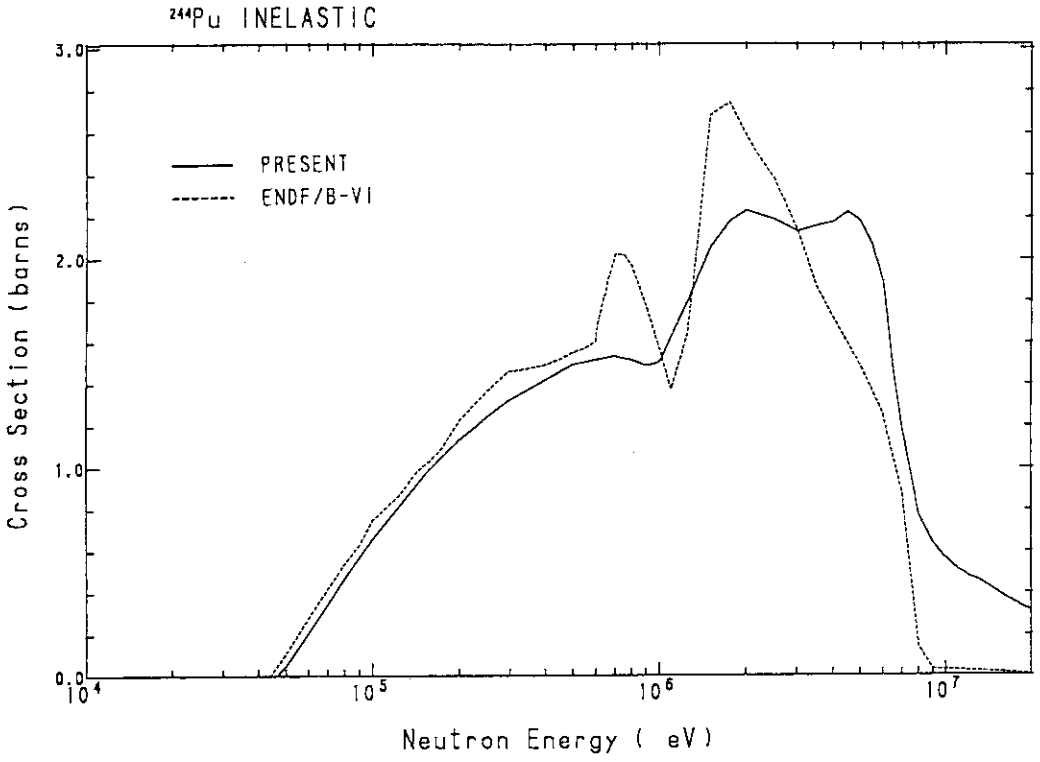


Fig.2.8 $^{244}$Pu total inelastic scattering cross section

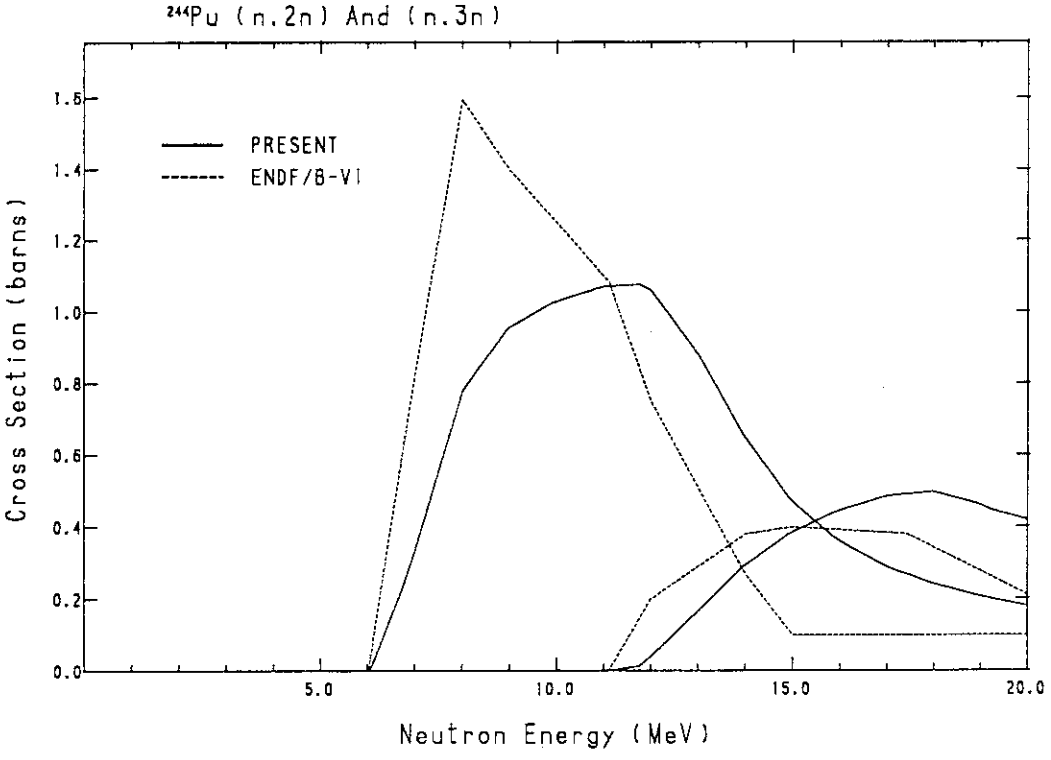


Fig.2.9 $^{244}$Pu(n,2n) and (n,3n) reaction cross sections

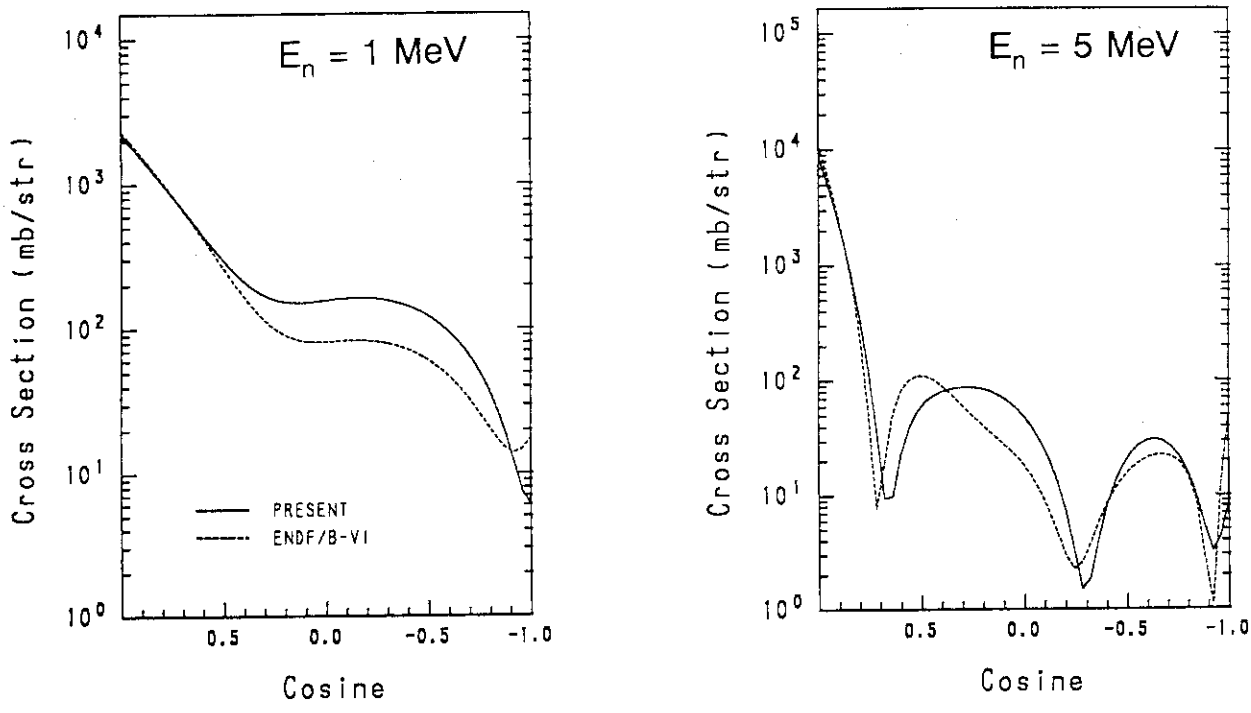


Fig.2.10(a) Angular distributions of elastically scattered neutrons from $^{244}Pu$

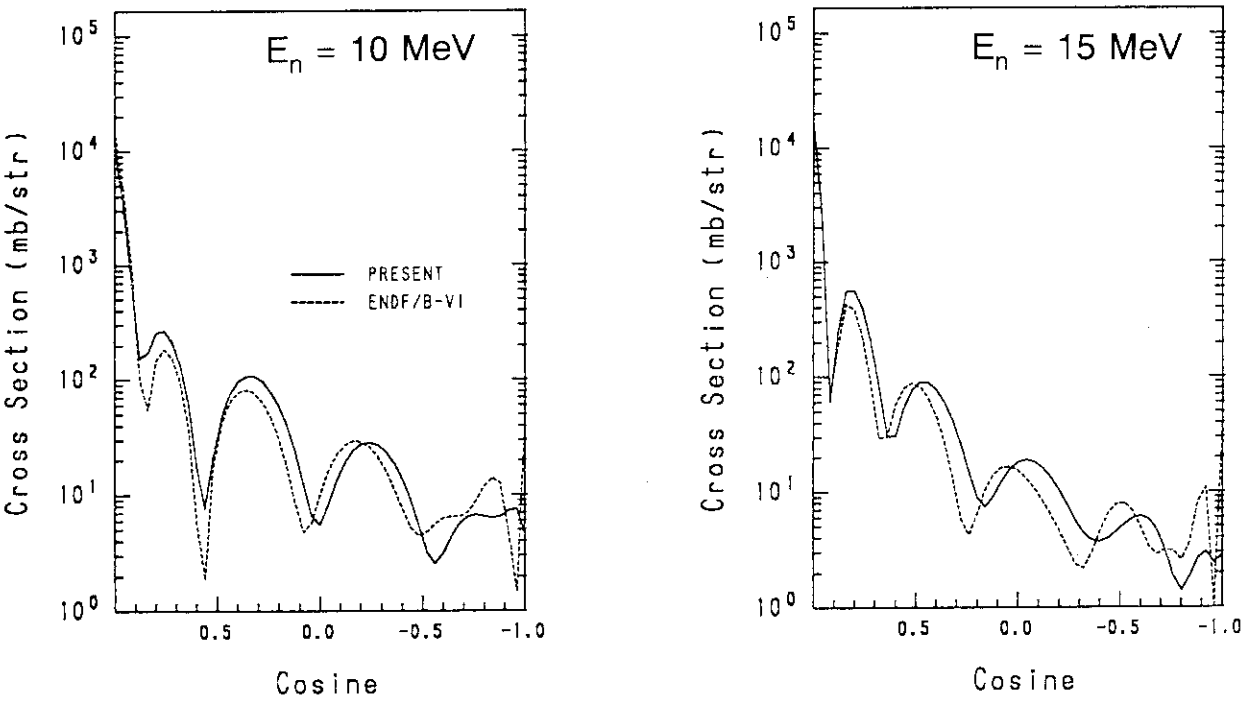


Fig.2.10(b) Angular distributions of elastically scattered neutrons from $^{244}Pu$

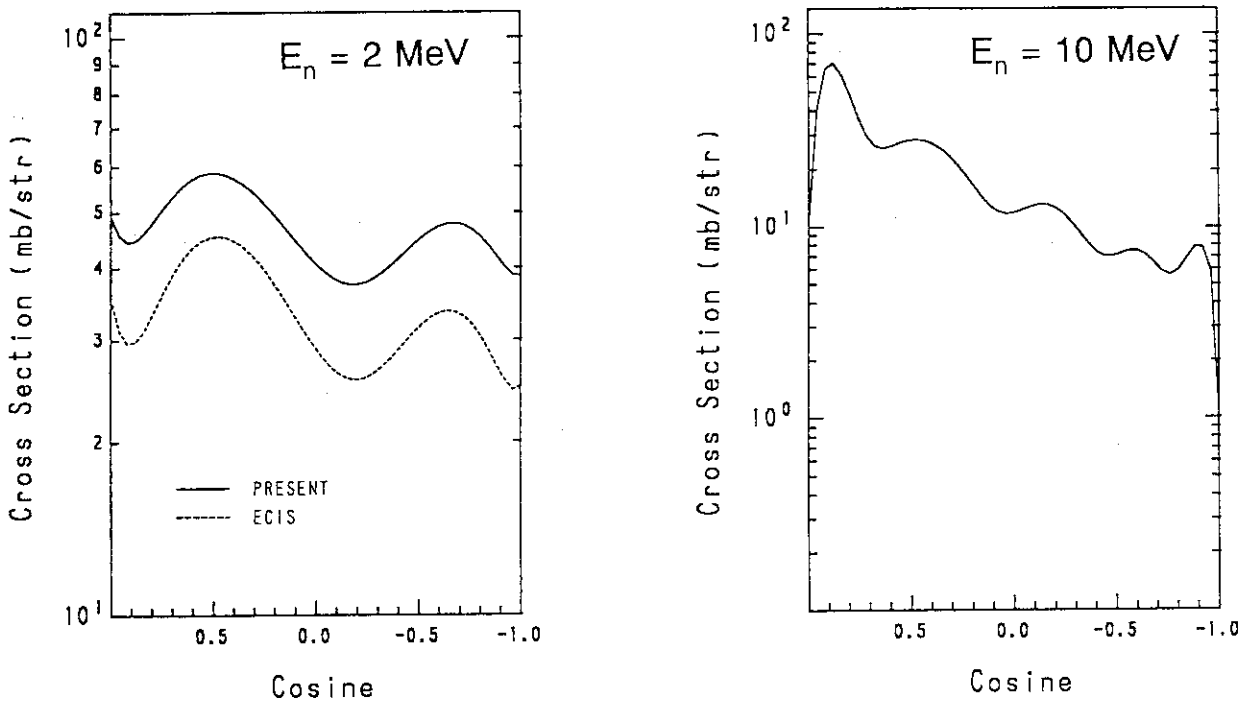


Fig.2.11 Angular distributions of inelastically scattered neutrons from $^{244}$Pu 48-keV level. The solid line shows the present result, and the dashed one the result of ECIS calculation. At 10 MeV, the both are the same.

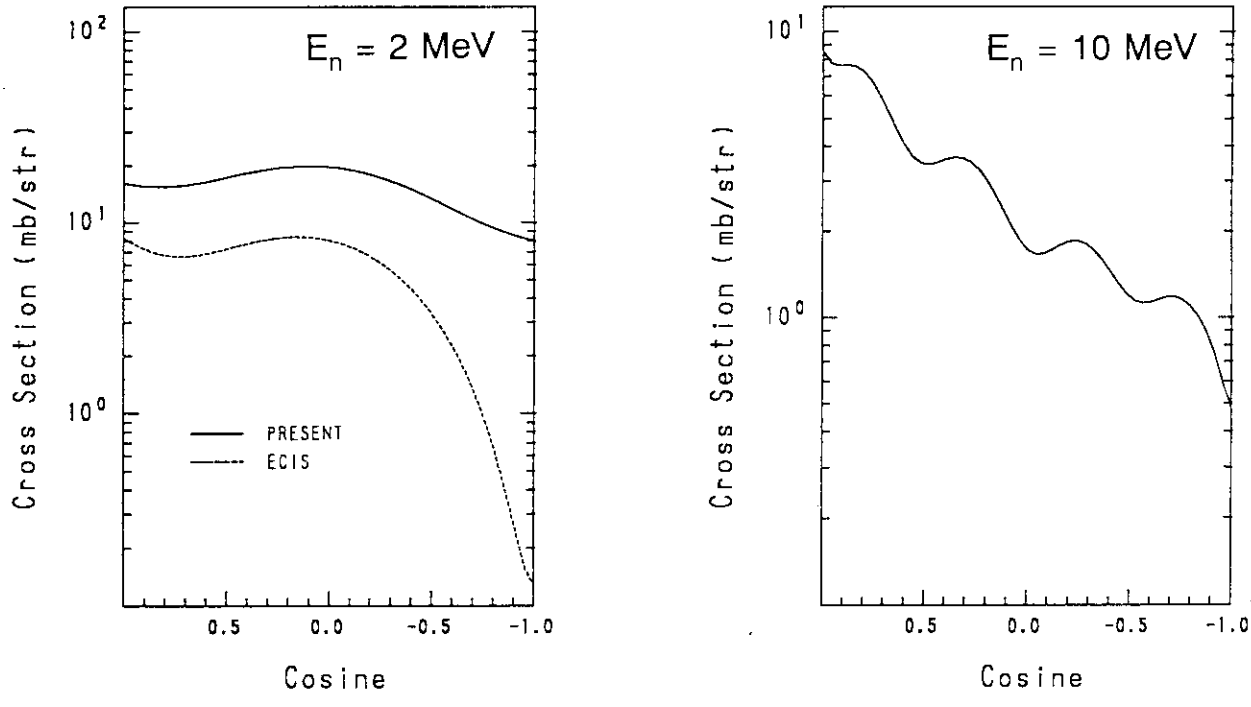


Fig.2.12 Angular distributions of inelastically scattered neutrons from $^{244}$Pu 153-keV level (See Fig.2.11)

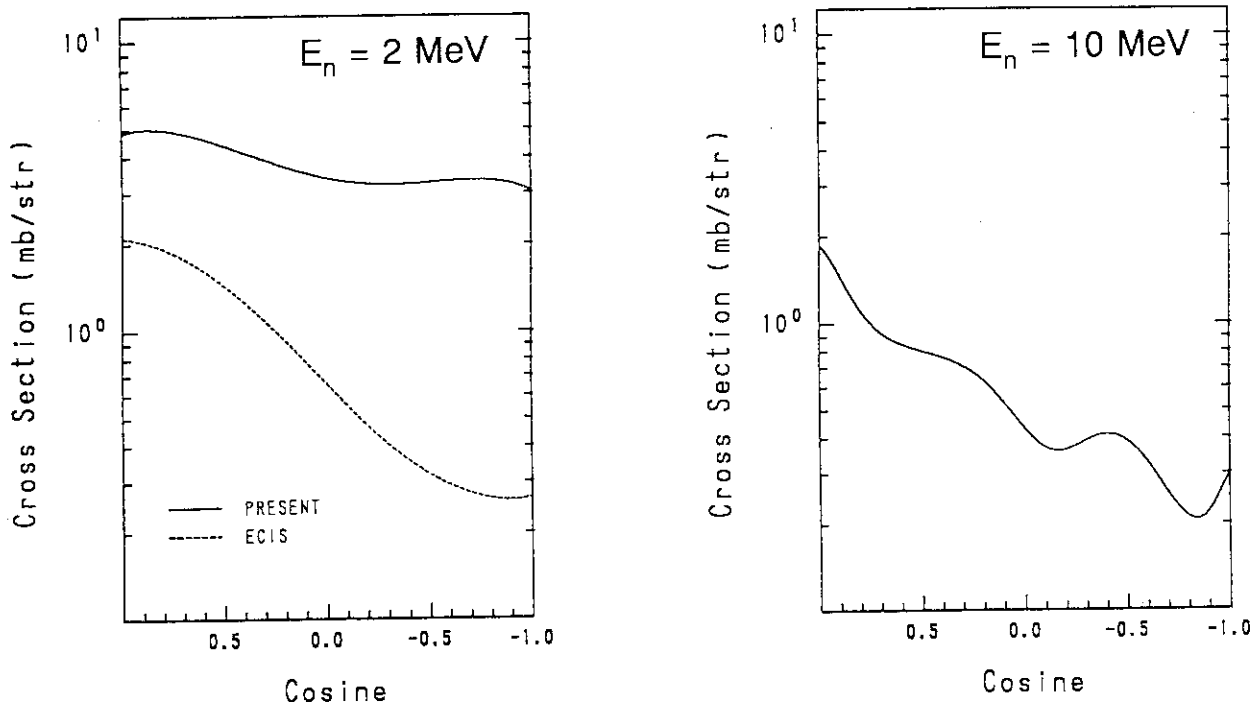


Fig.2.13 Angular distributions of inelastically scattered neutrons from $^{244}$Pu 315-keV level (See Fig.2.11)

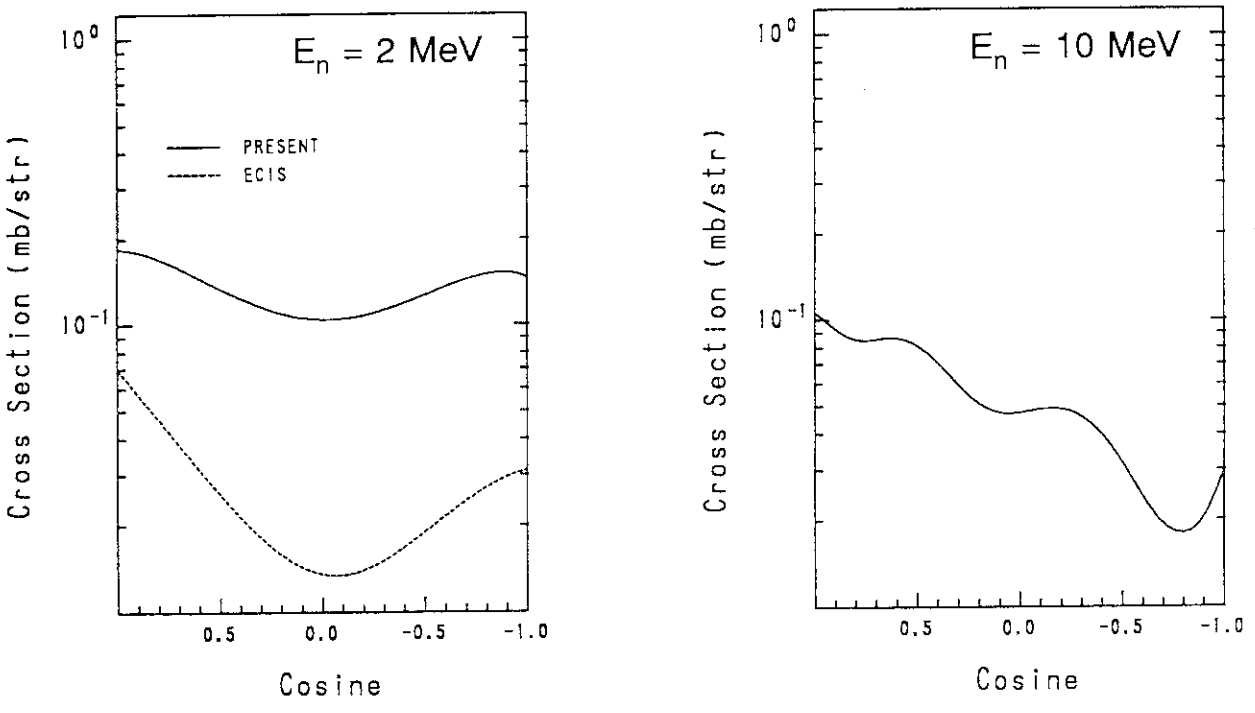


Fig.2.14 Angular distributions of inelastically scattered neutrons from $^{244}$Pu 532-keV level (See Fig.2.11)

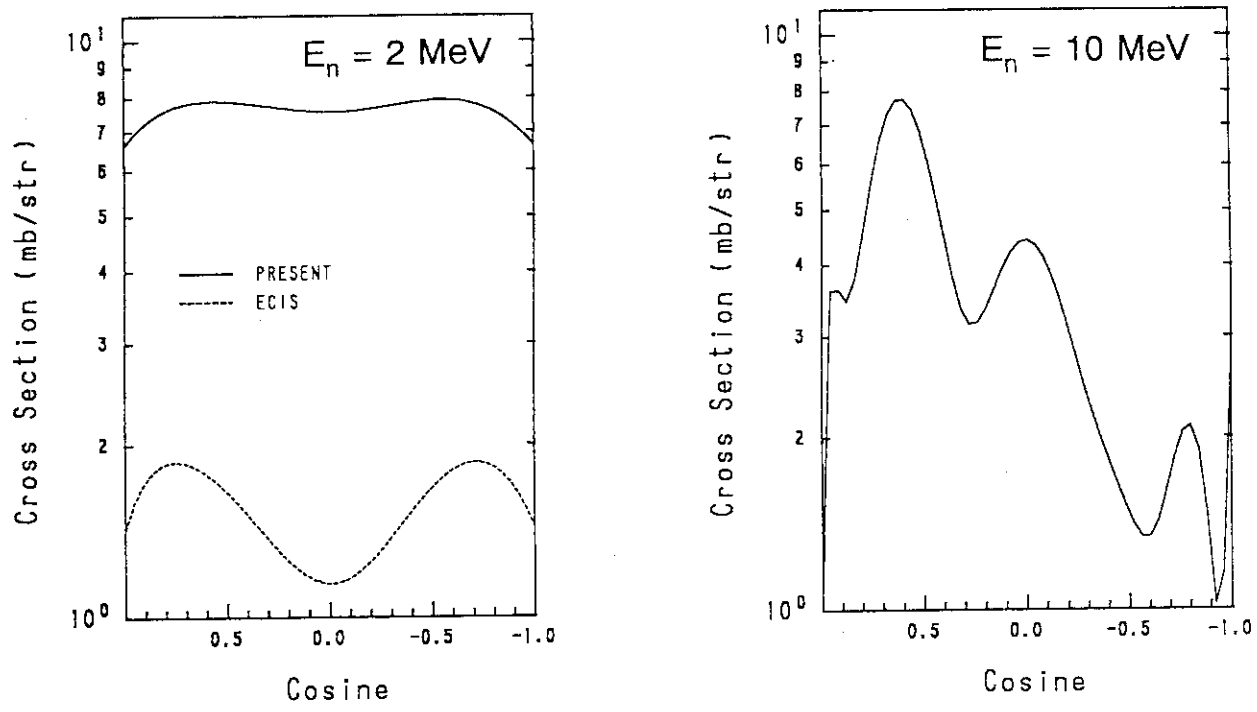


Fig.2.15 Angular distributions of inelastically scattered neutrons from $^{244}$Pu 708-keV level (See Fig.2.11)

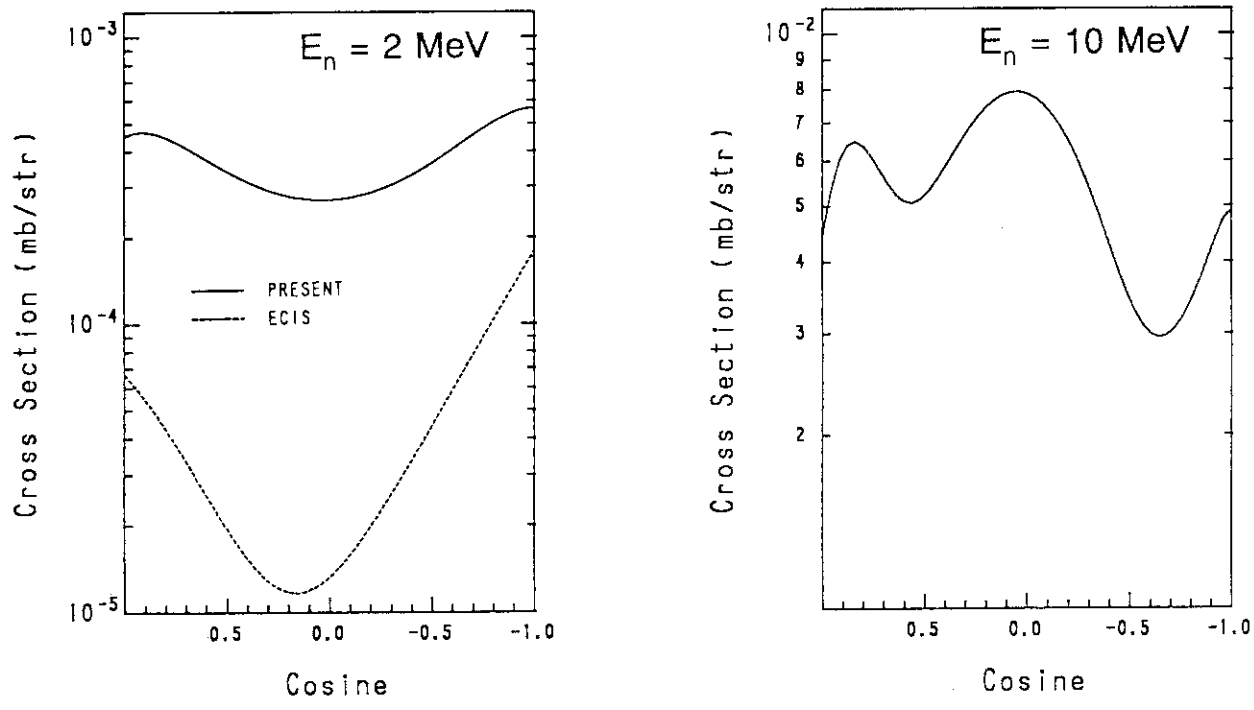


Fig.2.16 Angular distributions of inelastically scattered neutrons from $^{244}$Pu 798-keV level (See Fig.2.11)

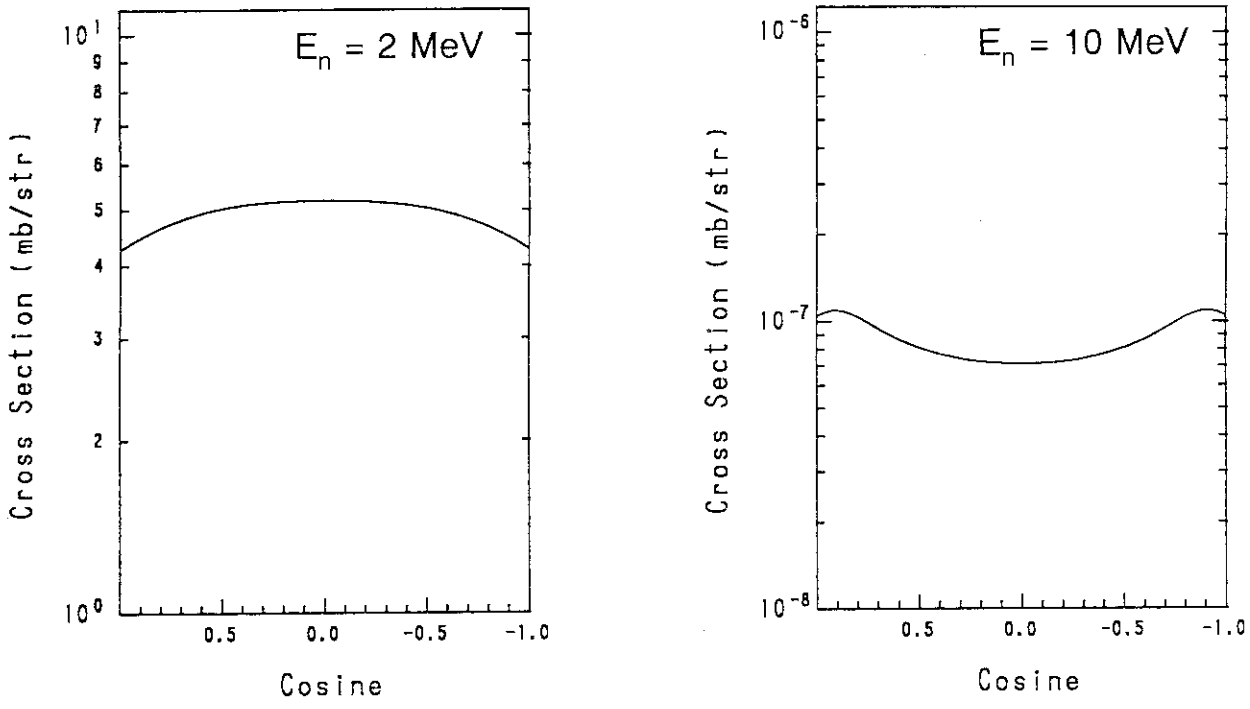


Fig.2.17 Angular distributions of inelastically scattered neutrons from $^{244}$Pu 957-keV level

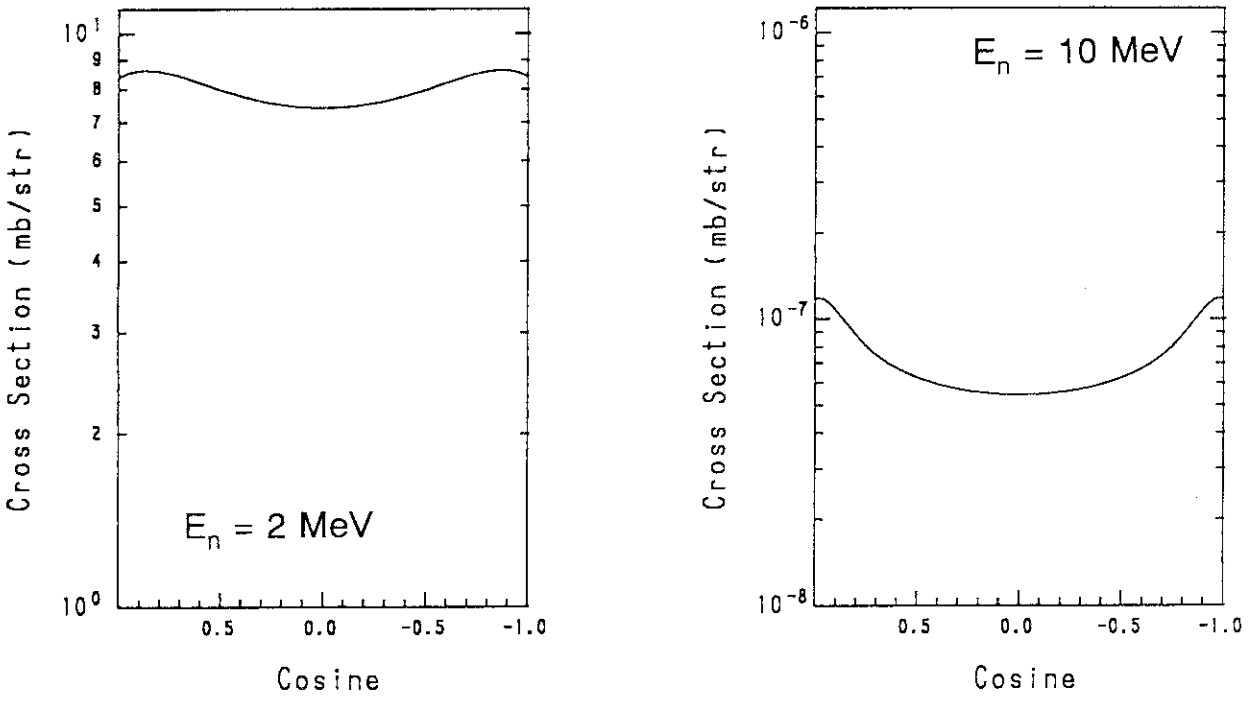


Fig.2.18 Angular distributions of inelastically scattered neutrons from $^{244}$Pu 1015-keV level

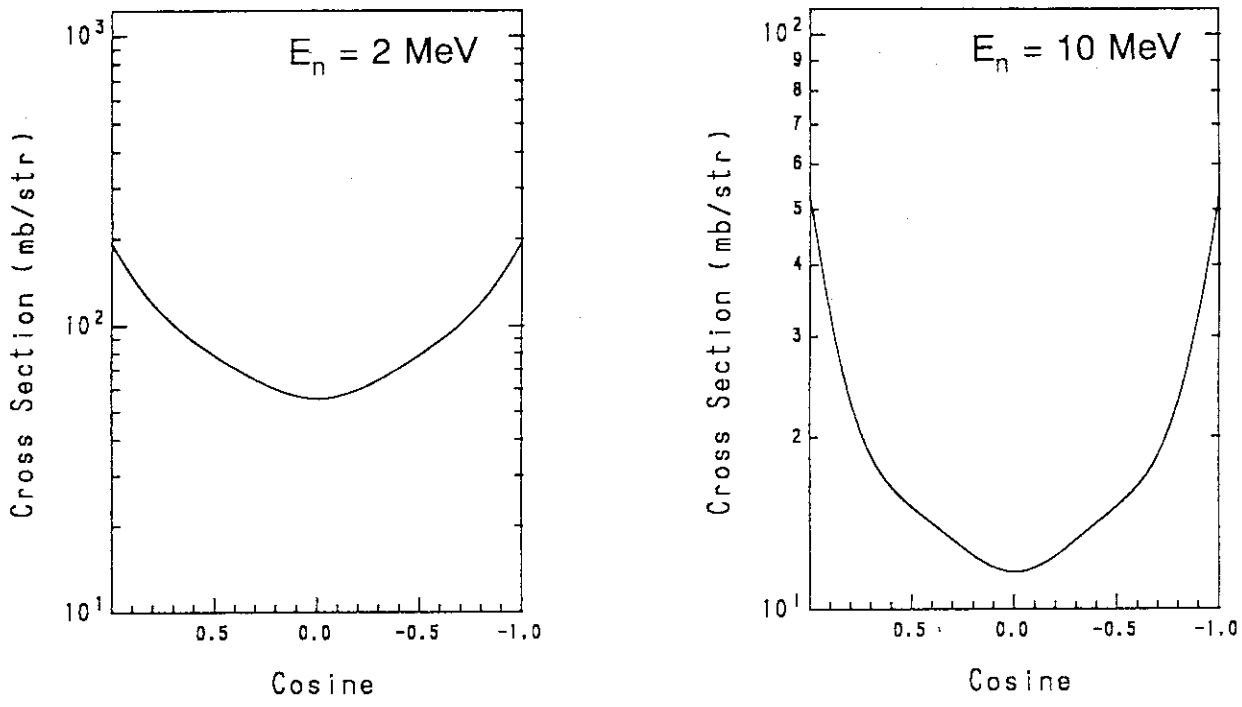


Fig.2.19 Angular distributions of inelastically scattered neutrons from $^{244}$Pu continuum level

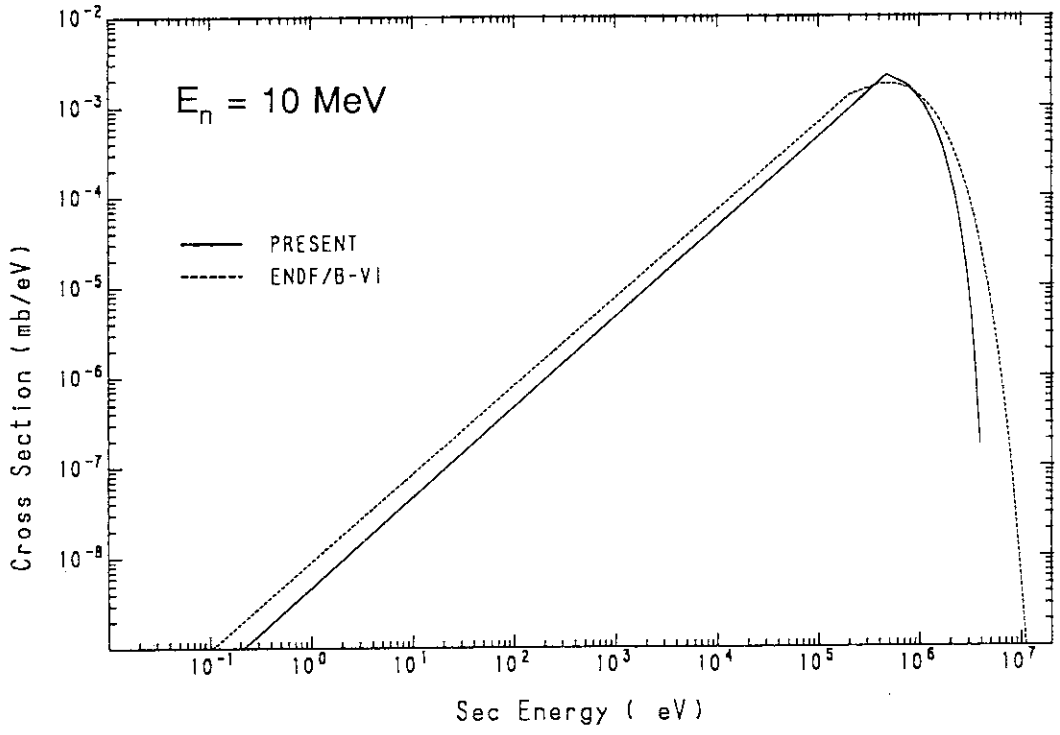


Fig.2.20 Energy distributions of neutrons emitted from $^{244}$Pu (n,2n) reaction at 10 MeV

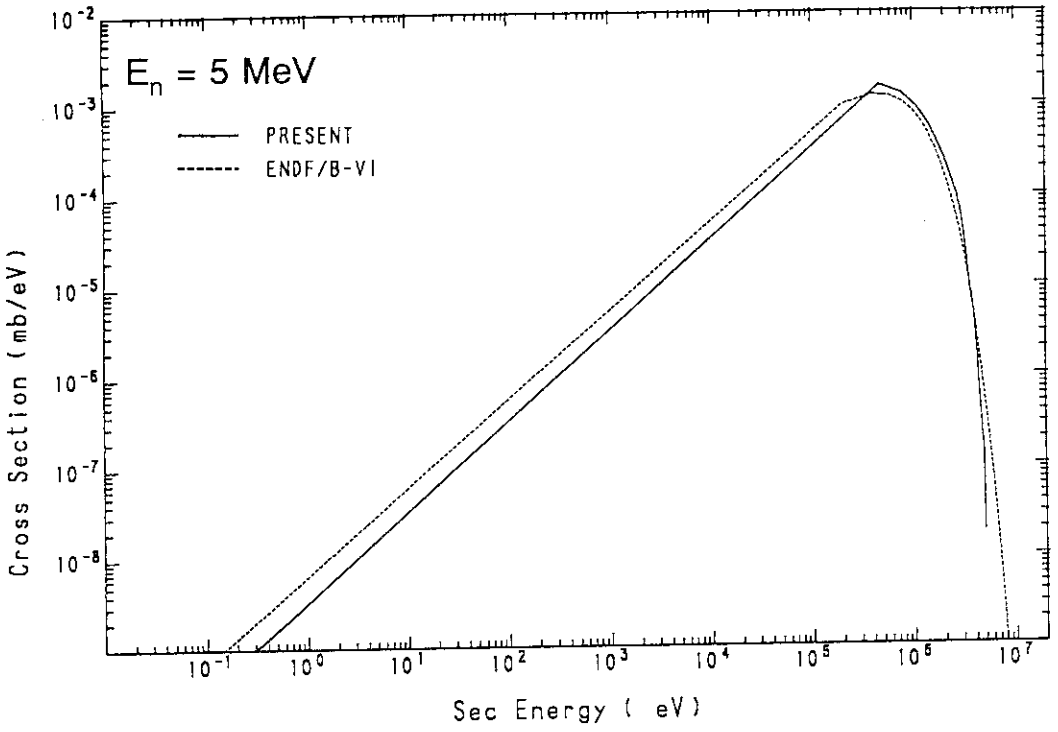


Fig.2.21 Energy distributions of neutrons emitted from $^{244}$Pu continuum inelastic scattering at 5 MeV

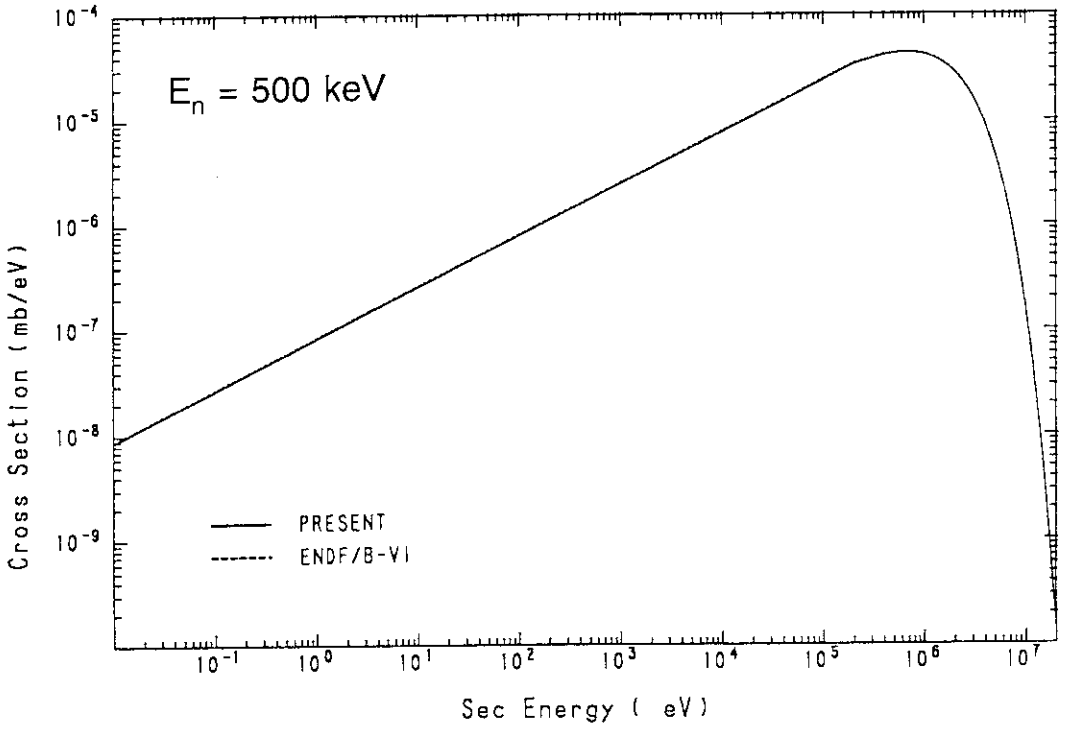


Fig.2.22 Energy distributions of $^{244}$Pu fission neutrons ($E_n$=500 keV)

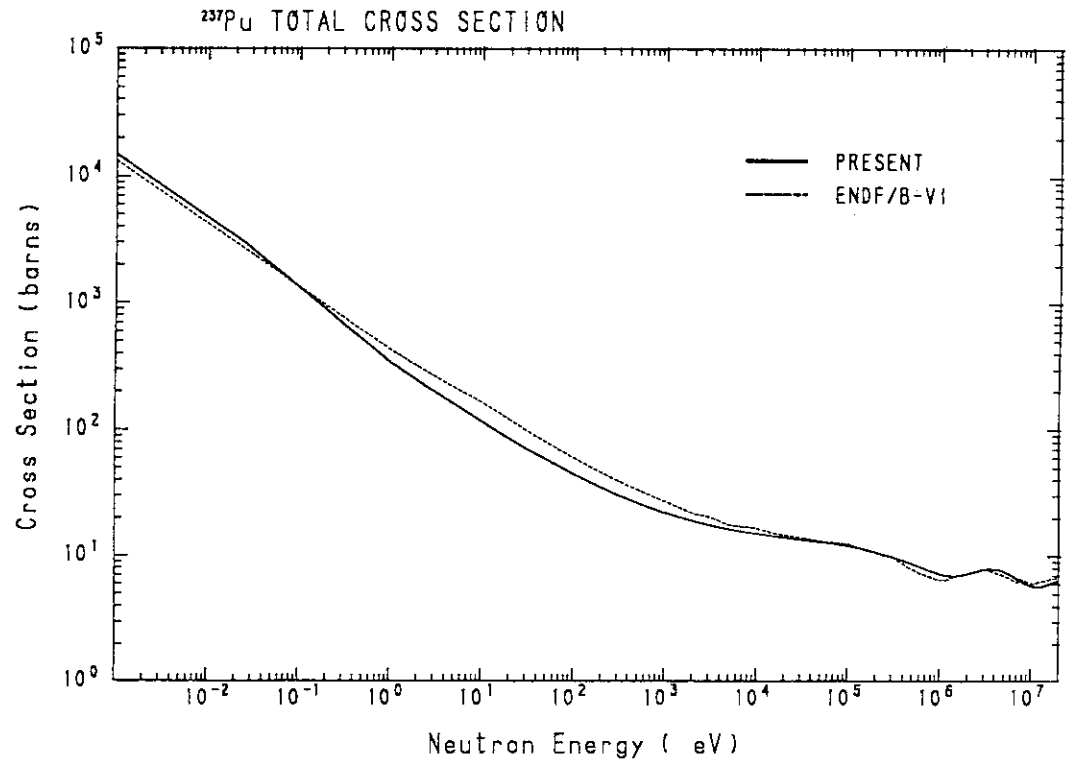


Fig.3.1 $^{237}$Pu total cross section

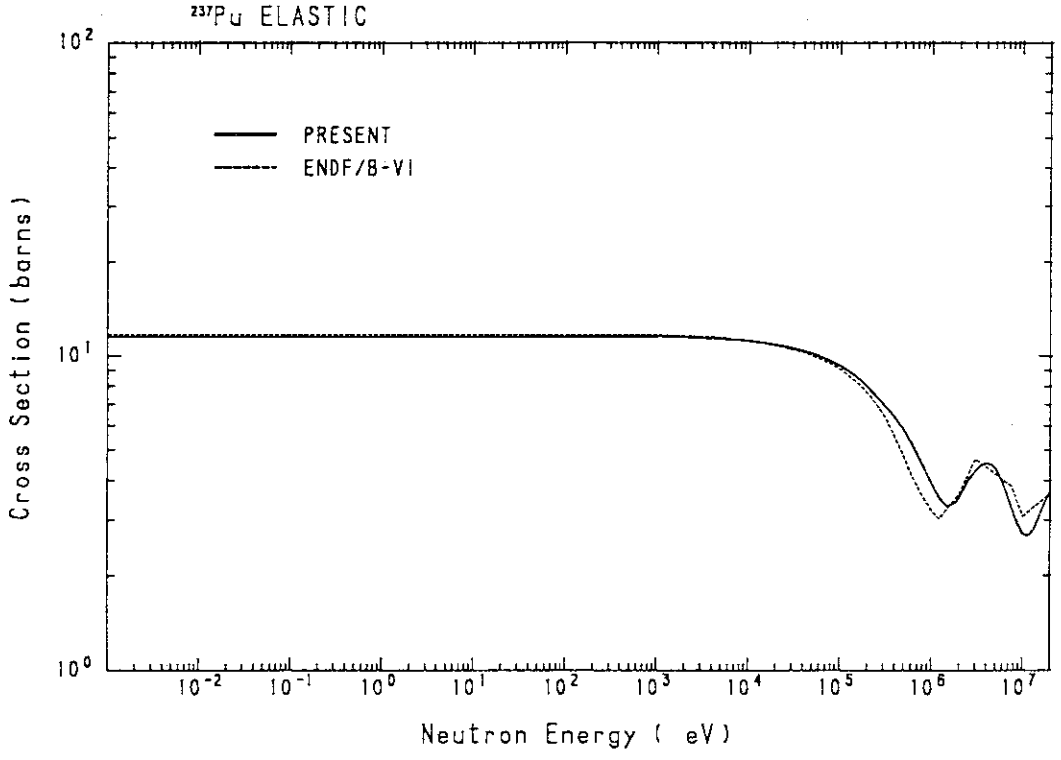


Fig.3.2 $^{237}$Pu elastic scattering cross section

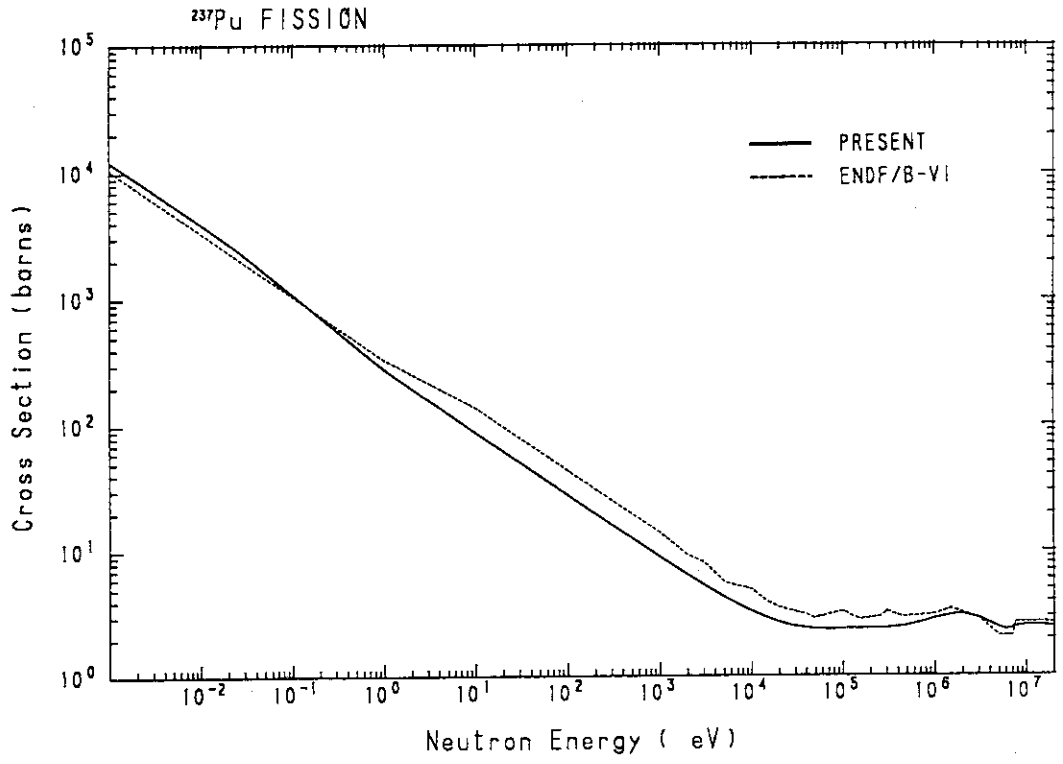


Fig.3.3 $^{237}$Pu fission cross section

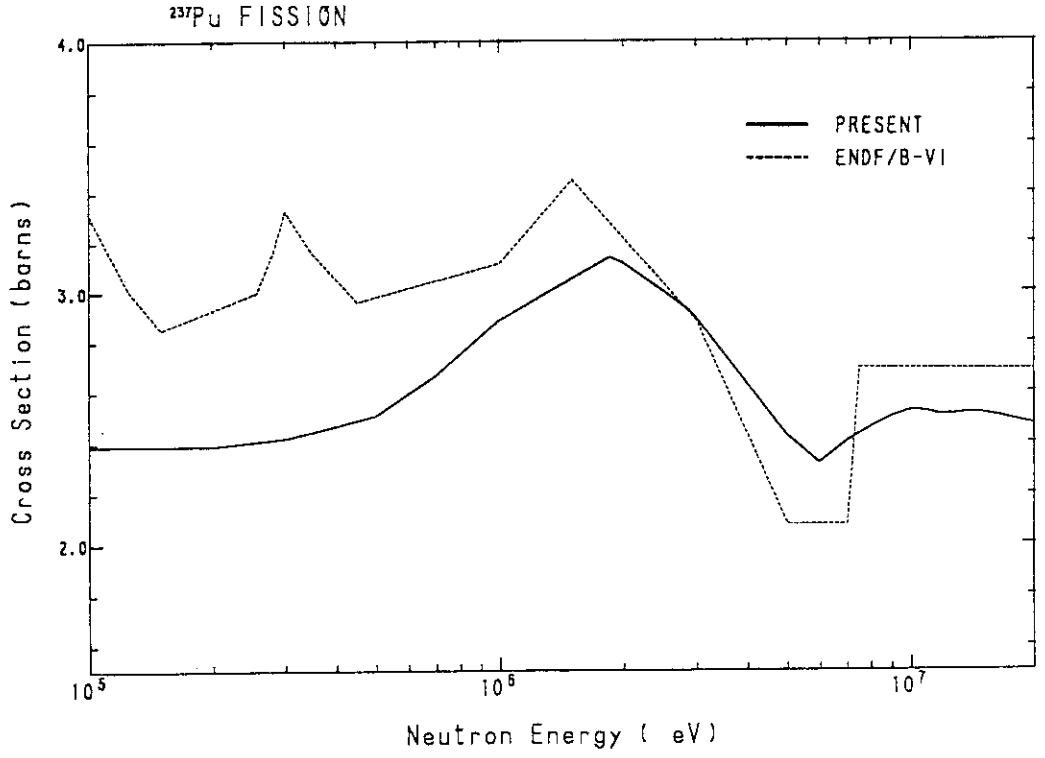


Fig.3.4 $^{237}$Pu Fisson cross section (Above 100 keV)

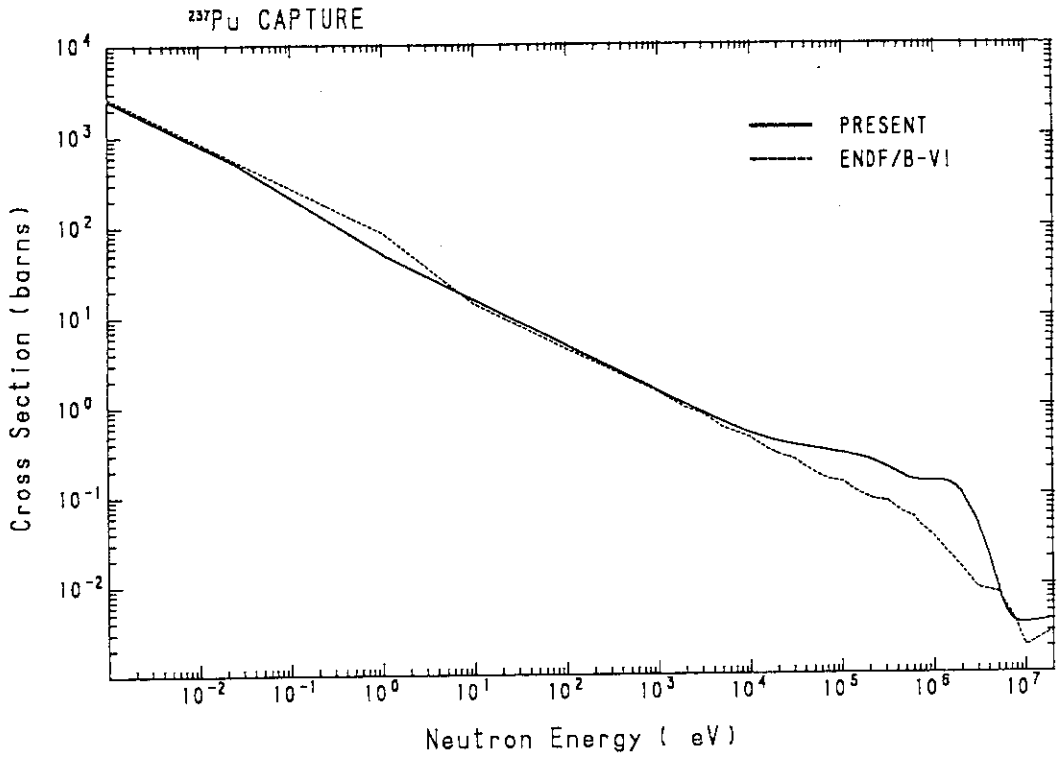


Fig.3.5 $^{237}$Pu capture cross section

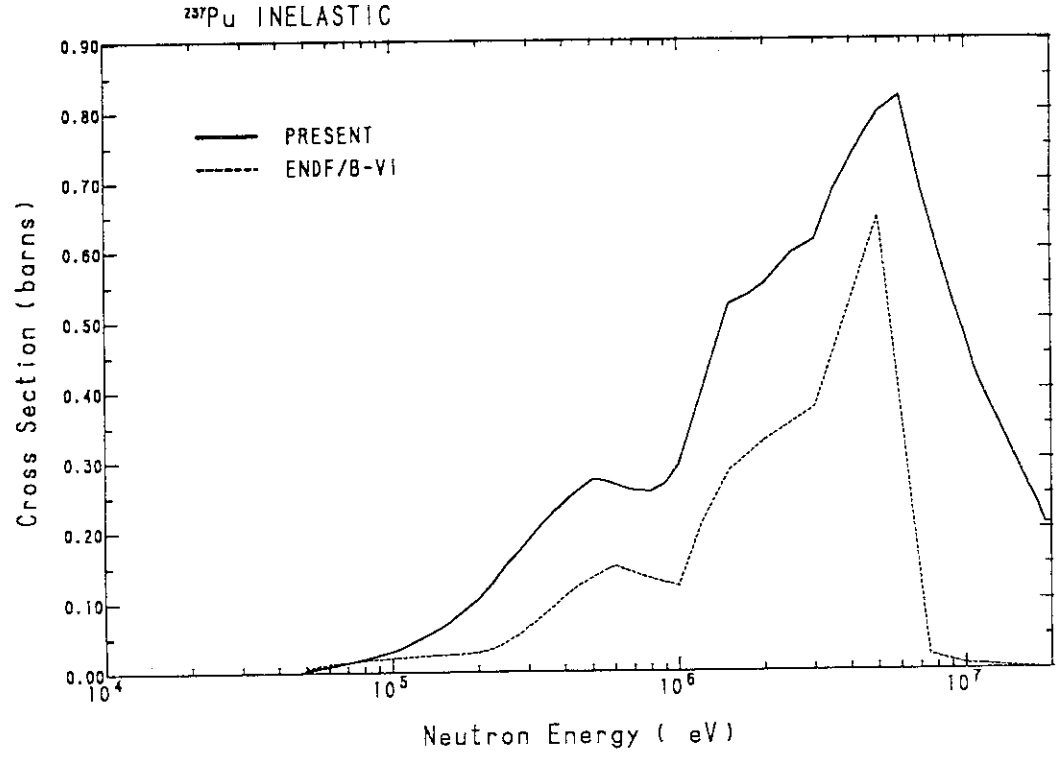


Fig.3.6 $^{237}$Pu total inelastic scattering cross section

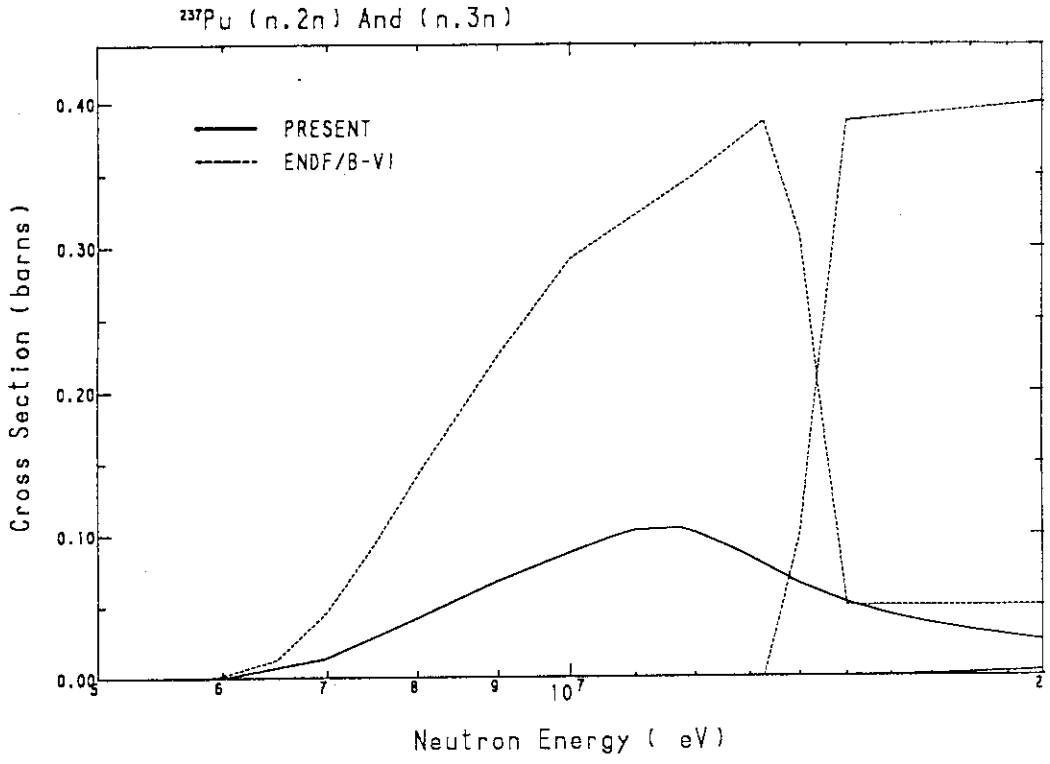


Fig.3.7 $^{237}Pu$ (n,2n) and (n,3n) reaction cross sections

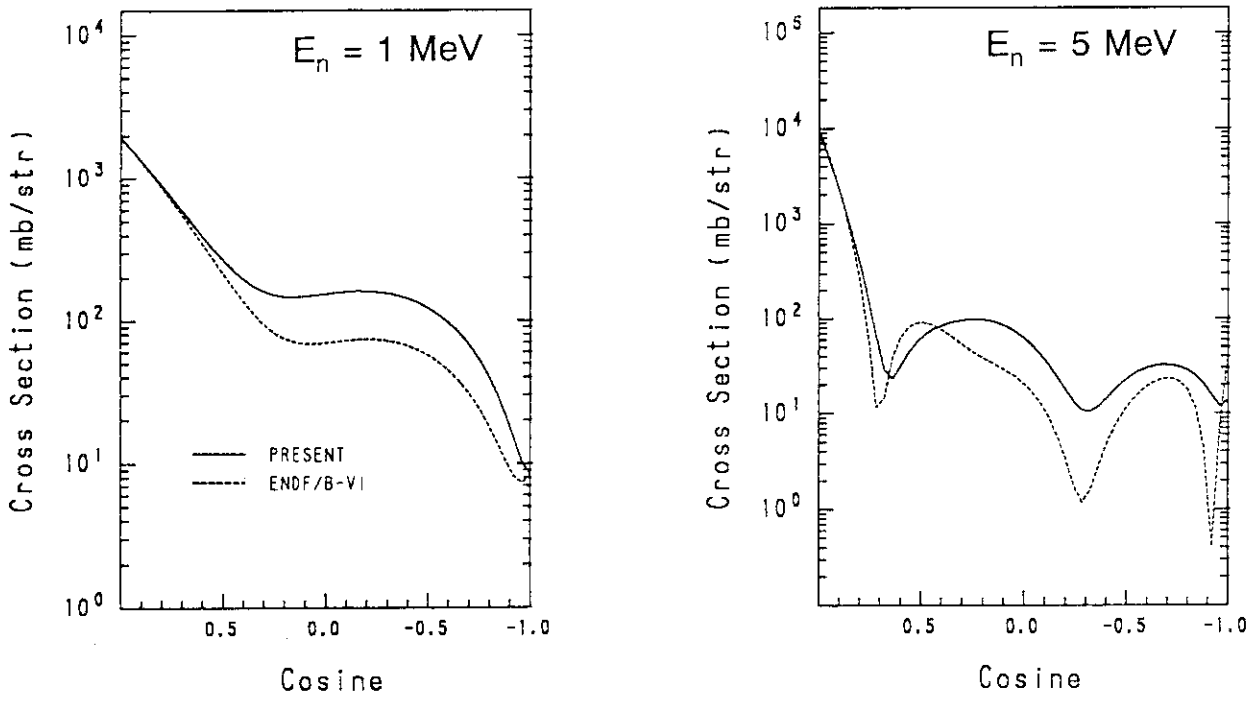


Fig.3.8(a) Angular distributions of elastically scattered neutrons from $^{237}Pu$

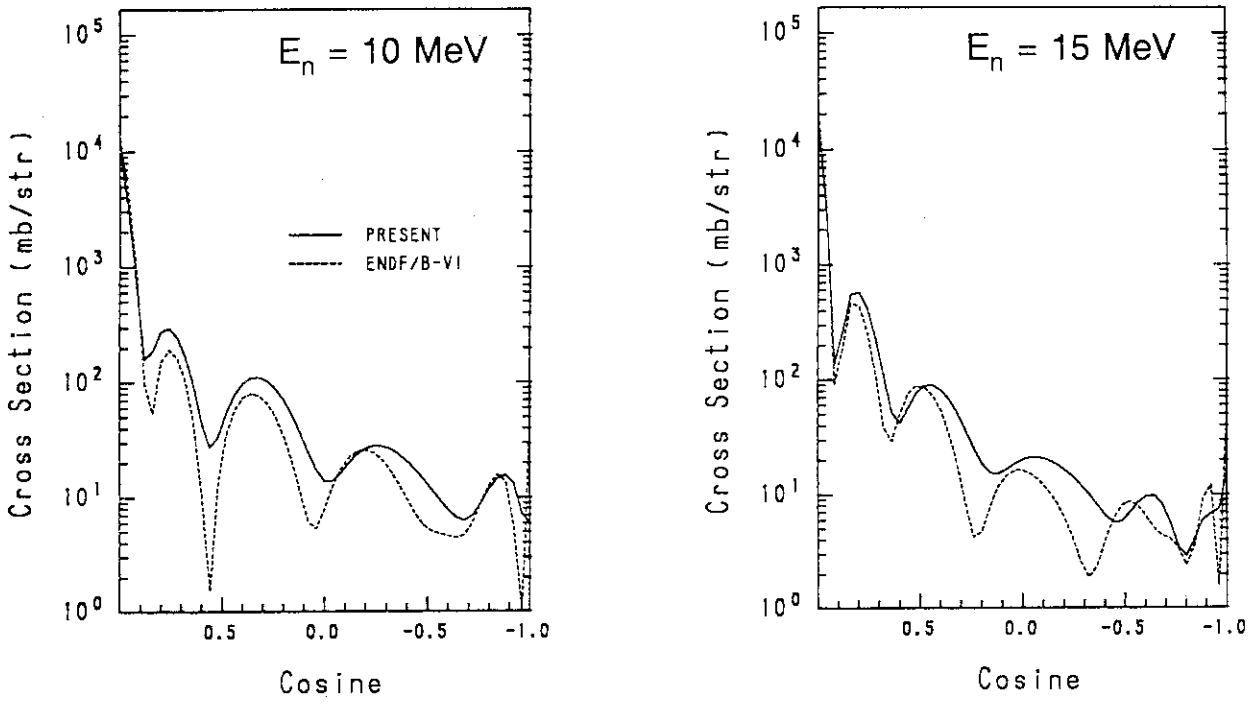


Fig.3.8(b) Angular distributions of elastically scattered neutrons from $^{237}$Pu

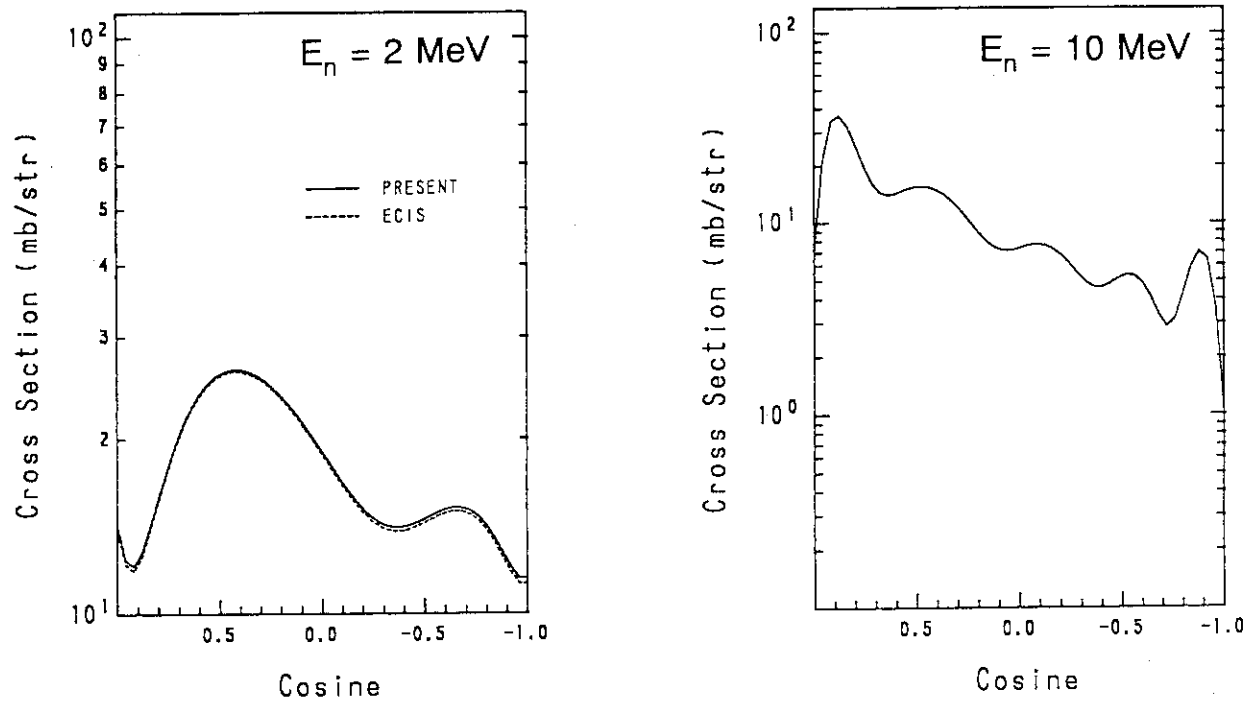


Fig.3.9 Angular distributions of inelastically scattered neutrons from $^{237}$Pu 48-keV level

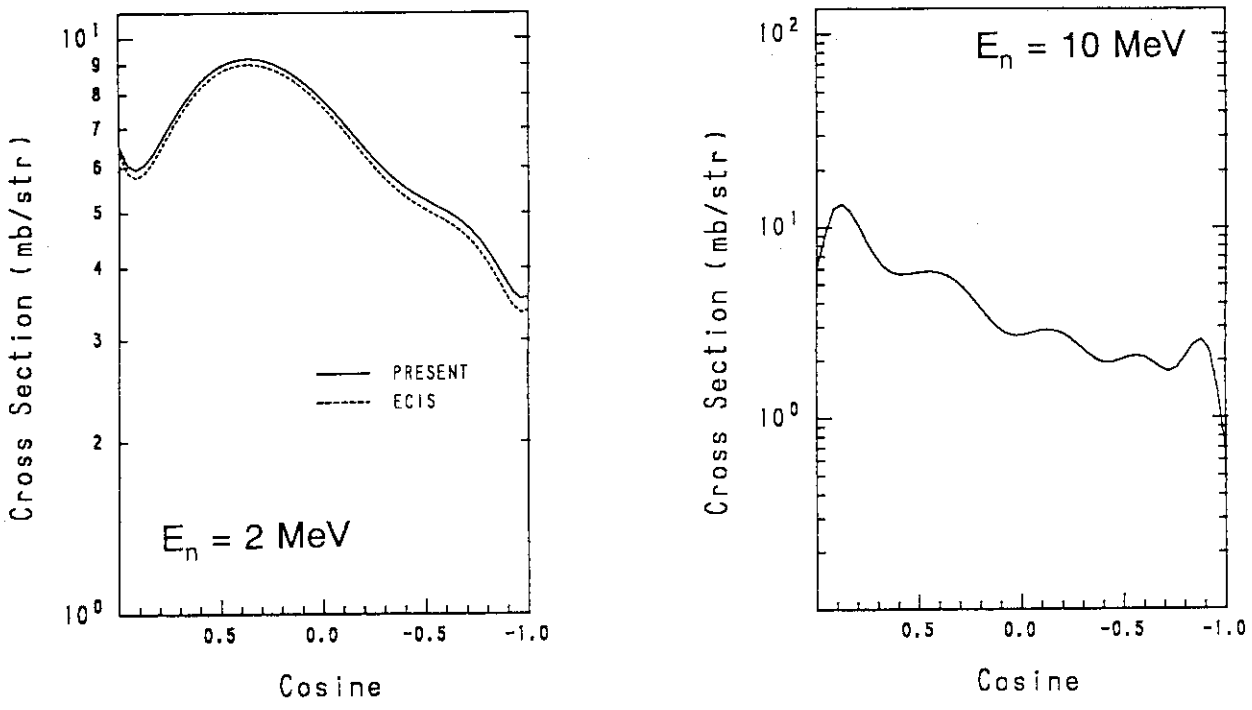


Fig.3.10 Angular distributions of inelastically scattered neutrons from $^{237}$Pu 106-keV level

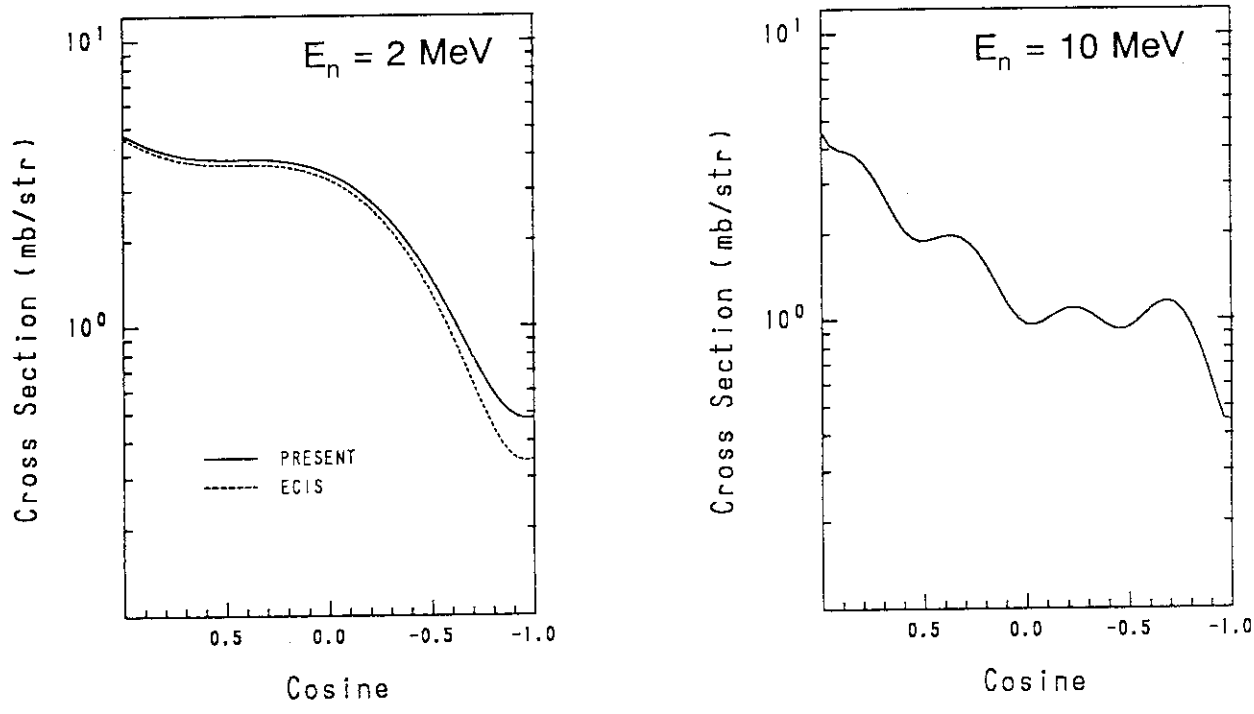


Fig.3.11 Angular distributions of inelastically scattered neutrons from $^{237}$Pu 175-keV level

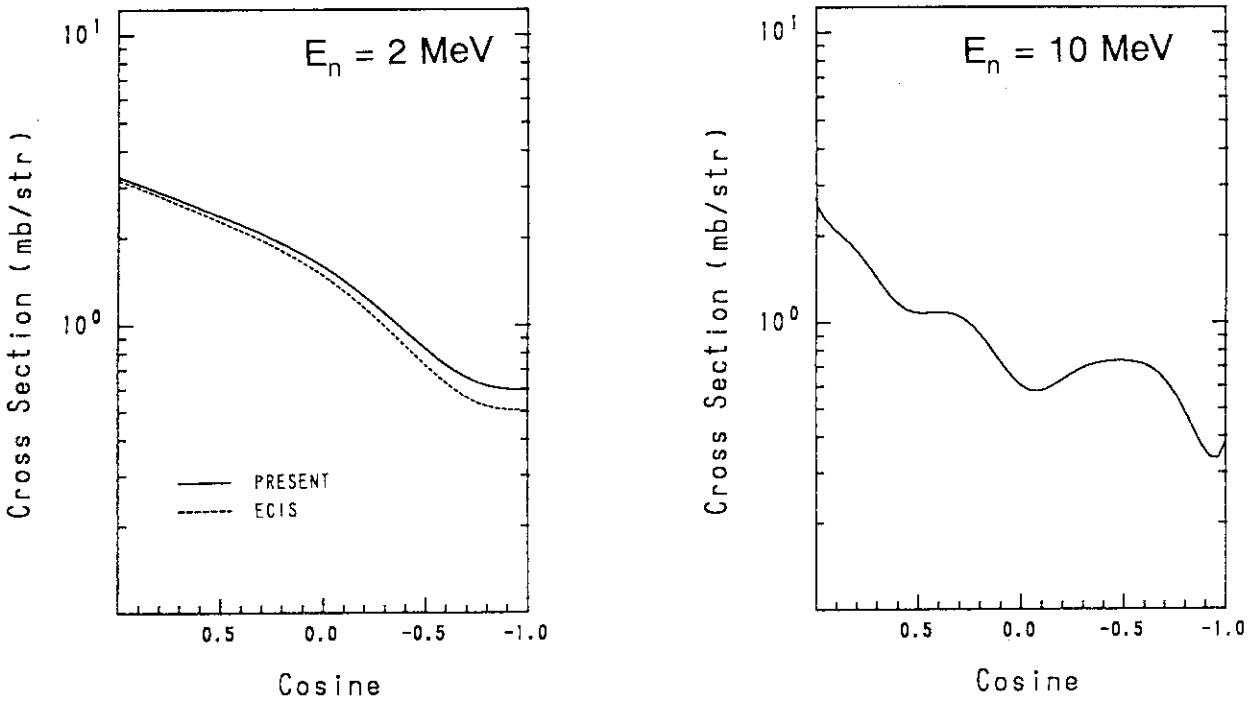


Fig.3.12 Angular distributions of inelastically scattered neutrons from $^{237}$Pu 257-keV level

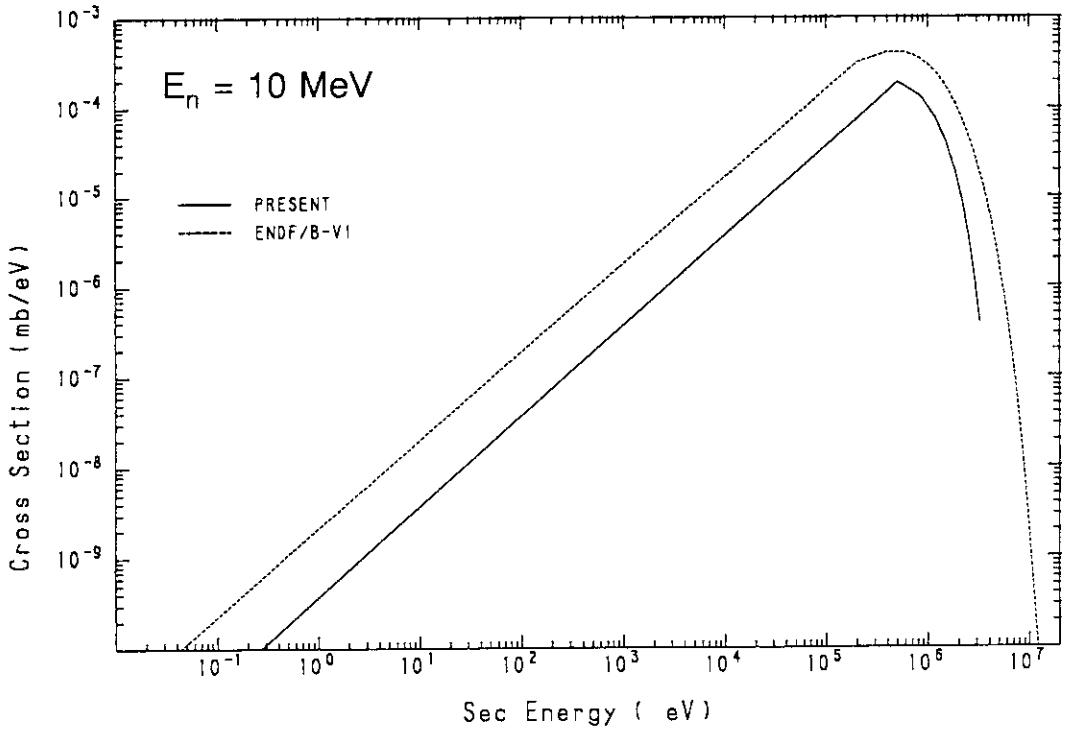


Fig.3.13 Energy distributions of neutrons emitted from $^{237}$Pu(n,2n) reaction at 10 MeV

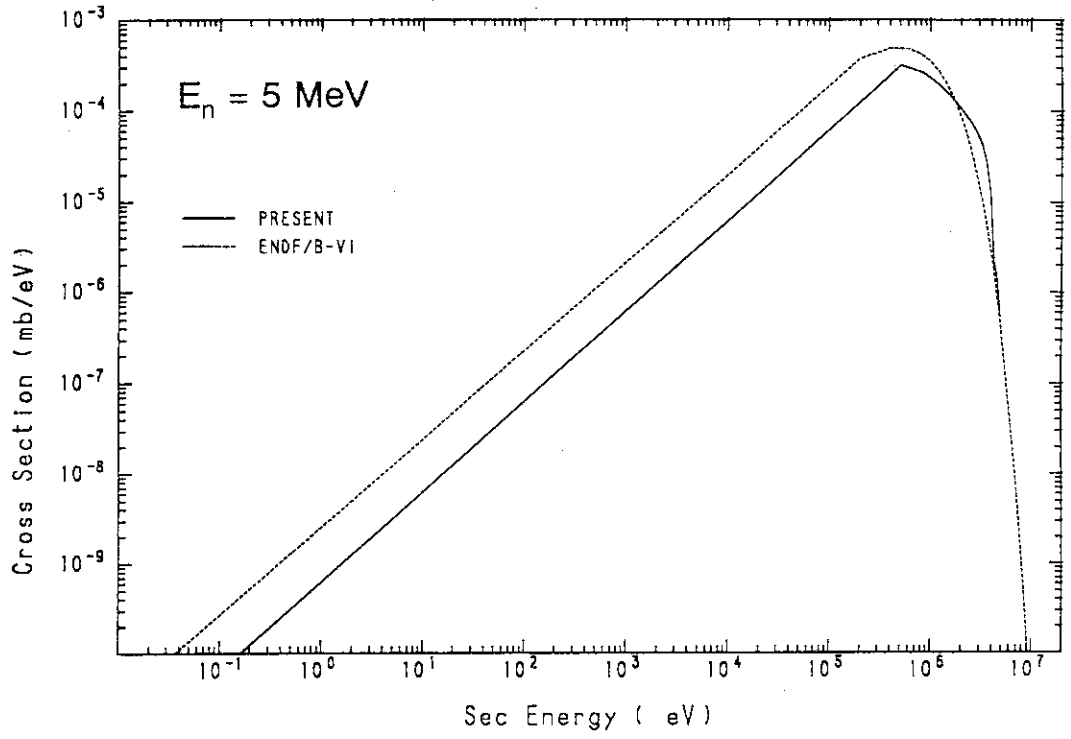


Fig.3.14 Energy distributions of neutrons emitted from $^{237}$Pu continuum inelastic scattering at 5 MeV

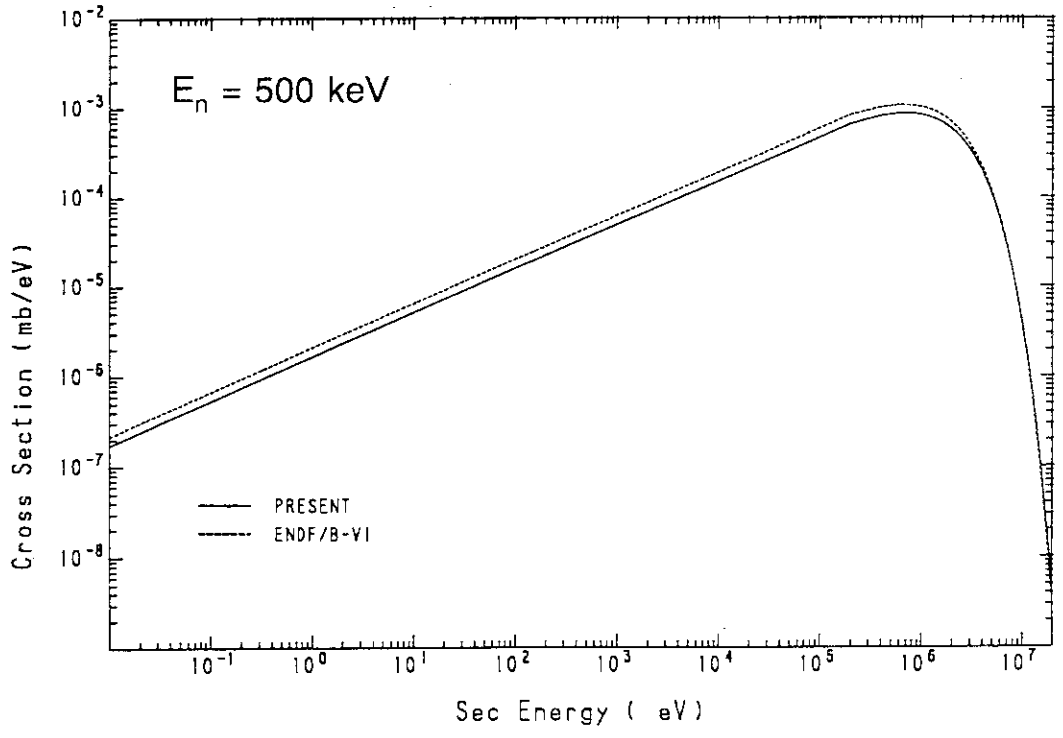


Fig.3.15 Energy distributions of $^{237}$Pu fission neutrons ($E_n$=500 keV)